J Membrane Biol (2007) 220:33–51
DOI 10.1007/s00232-007-9073-5

Turnover Rate of the γ-Aminobutyric Acid Transporter GAT1

Albert L. Gonzales · William Lee · Shelly R. Spencer · Raymond A. Oropeza · Jacqueline V. Chapman · Jerry Y. Ku · Sepehr Eskandari

Received: 20 June 2007 / Accepted: 14 September 2007 / Published online: 9 November 2007

Abstract We combined electrophysiological and freeze-fracture methods to estimate the unitary turnover rate of the γ-aminobutyric acid (GABA) transporter GAT1. Human GAT1 was expressed in *Xenopus laevis* oocytes, and individual cells were used to measure and correlate the macroscopic rate of GABA transport and the total number of transporters in the plasma membrane. The two-electrode voltage-clamp method was used to measure the transporter-mediated macroscopic current evoked by GABA (I_{NaCl}^{GABA}), macroscopic charge movements (Q_{NaCl}) evoked by voltage pulses and whole-cell capacitance. The same cells were then examined by freeze-fracture and electron microscopy in order to estimate the total number of GAT1 copies in the plasma membrane. GAT1 expression in the plasma membrane led to the appearance of a distinct population of 9-nm freeze-fracture particles which represented GAT1 dimers. There was a direct correlation between Q_{NaCl} and the total number of transporters in the plasma membrane. This relationship yielded an apparent valence of 8 ± 1 elementary charges per GAT1 particle. Assuming that the monomer is the functional unit, we obtained 4 ± 1 elementary charges per GAT1 monomer. This information and the relationship between I_{NaCl}^{GABA} and Q_{NaCl} were used to estimate a GAT1 unitary turnover rate of 15 ± 2 s^{-1} (21°C, −50 m*V*). The temperature and voltage dependence of GAT1 were used to estimate the physiological turnover rate to be 79–93 s^{-1} (37°C, −50 to −90 m*V*).

Keywords Sodium-coupled transport · Neurotransmitter transporter · GABA · GAT1 · Turnover rate · Freeze-fracture

A. L. Gonzales · W. Lee · S. R. Spencer · R. A. Oropeza · J. V. Chapman · J. Y. Ku · S. Eskandari (✉)
Biological Sciences Department, California State Polytechnic University, 3801 West Temple Avenue, Pomona, CA 91768-4032, USA
e-mail: seskandari@csupomona.edu

Present Address:
A. L. Gonzales
Department of Biomedical Sciences, College of Veterinary Medicine and Biomedical Sciences, Colorado State University, Fort Collins, CO 80523, USA

Present Address:
W. Lee
Department of Cell Biology and Neuroscience, University of California, Riverside, CA 92521, USA

Introduction

γ-Aminobutyric acid (GABA) transporters (GATs) are responsible for maintaining low resting levels of GABA in the central nervous system, as well as for modulating synaptic and extrasynaptic GABAergic neurotransmission (Borden, 1996; Nelson, 1998; Dalby, 2003; Richerson & Wu, 2003; Conti, Minelli & Melone, 2004). An important factor that governs the ability of the GATs to shape fast synaptic events, such as those mediated by $GABA_A$ receptors, is the rate at which these proteins transport GABA across the plasma membrane per unit time (i.e., turnover rate). For the forward mode of transport (Na^+/Cl^-/GABA cotransport into the cell), estimates of the turnover rate range 1.5–25 s^{-1} at 21–23°C and voltages ranging from −50 to −120 m*V* (Radian, Bendahan & Kanner, 1986; Mager et al., 1993; Forlani et al., 2001b; Fesce et al., 2002; Sacher et al., 2002; Whitlow et al., 2003; Karakossian et al., 2005). For the reverse mode, the turnover rate has been estimated to range 3–60 s^{-1} at 33°C, and voltages ranging from −120 to +120 m*V* (Lu & Hilgemann, 1999b).

Given that the turnover rate is subject to physiological and pharmacological regulation (Deken et al., 2000; Quick, 2002; Wang et al., 2003; Whitlow et al., 2003; Hansra, Arya & Quick, 2004), a reliable estimate of the transporter turnover rate is needed for a full understanding of GAT physiology and pathophysiology.

Three factors limit the utility of the turnover rate estimates noted above. (1) Turnover rate estimates have relied exclusively on electrophysiological methods for determining the number of GAT1 molecules in the plasma membrane. While these methods are powerful, they may suffer from a number of intrinsic assumptions whose validity must be established independently. (2) Most studies have determined the turnover rate at room temperature (20–23°C), far from the physiological temperature (37°C) at which these proteins perform their normal function. The high temperature dependence of the GATs necessitates that the measurements be performed at 37°C or in a way to ensure reliable extrapolation to the physiological temperature (Binda et al., 2002; Karakossian et al., 2005). (3) Most turnover rate measurements have been done at nonphysiological ion concentrations used in experiments on *Xenopus laevis* oocytes expressing the GATs with no attempt to quantitatively account for these deviations. The goal of the present study was to closely examine the three above-mentioned limitations in order to provide a reliable estimate of the physiological turnover rate of GAT1.

The standard approach for determining the turnover rate has been to use electrophysiological methods in *X. laevis* oocytes expressing the GATs. The turnover rate is estimated by obtaining the ratio of the maximum GABA-evoked inward current (I_{max}) and the maximum voltage-induced transporter charge movements (Q_{max}) (Loo et al., 1993; Mager et al., 1993; Lu & Hilgemann, 1999b; Forlani et al., 2001a,b; Fesce et al., 2002; Sacher et al., 2002; Karakossian et al., 2005). I_{max} is necessarily obtained under saturating substrate concentrations and is defined as $I_{max} = N_T meR_T$, where N_T is the total number of functional transporters in the plasma membrane, m is the number of charges translocated across the plasma membrane per transport cycle, e is the elementary charge and R_T is the unitary transporter turnover rate (cycles per second). The maximum charge (Q_{max}) moved in response to voltage pulses is obtained in the absence of GABA and is defined as $Q_{max} = N_T z\delta e$, where z is the valence of the moveable charge, δ is the fraction of the membrane electric field over which the charge moves and N_T and e have the same meaning as above. $z\delta$ is commonly referred to as the effective (or apparent) valence of the moveable charge. Because I_{max} is a measure of the maximal rate of GABA translocation across the plasma membrane (Loo et al., 2000; Sacher et al., 2002; Whitlow et al., 2003; Karakossian et al., 2005) and Q_{max} is proportional to the total number of transporters in the plasma membrane (Zampighi et al., 1995; Eskandari et al., 2000), the ratio of I_{max} to Q_{max} $[(N_T meR_T)/(N_T z\delta e)]$ has been used to estimate the GAT turnover rate (*see* Fig. 1d) (Mager et al., 1993; Forlani et al., 2001a,b; Fesce et al., 2002; Sacher et al., 2002; Karakossian et al., 2005) and other electrogenic Na^+-coupled transporters (Loo et al., 1993; Wadiche et al., 1995; Mackenzie et al., 1996; Eskandari et al., 1997; Forster et al., 2002; Mim et al., 2005).

It is readily seen that the approach described above is valid only if the following three criteria are met. (1) The substrate-evoked current must represent the maximum macroscopic current mediated by GAT1 (I_{max}). Thus, the cosubstrates (Na^+, Cl^-, GABA) must be present at saturating concentrations. (2) The voltage-induced transporter-mediated charge movements must represent the maximum macroscopic charge (Q_{max}). Thus, the cosubstrate needed for charge movement (Na^+) must be present at a saturating concentration and the test voltages must cover a wide enough range in order to estimate the true Q_{max}. (3) The number of charges translocated across the plasma membrane per transport cycle (m) must equal the apparent valence of the moveable charge ($z\delta$). The validity of these three criteria must be established experimentally for each transporter. Moreover, to estimate the physiological turnover rate, it is also necessary to define the turnover rate in terms of its dependence on temperature and membrane potential.

With the above considerations in mind, the goal of the present study was to provide a reliable estimate of the physiological turnover rate of GAT1. Although the GABA transporters are electrogenic, because turnover rates are so low, one cannot measure signals arising from single transporters, as is done in measuring unitary events of ion channels. Instead, the macroscopic signal from a large number of transporters must be measured and correlated with the known number of transporters giving rise to the measured macroscopic signal. This goal requires that the transporter be studied in a system in which both macroscopic transport rates and the number of transporters in the plasma membrane can be measured and correlated. We expressed the human isoform of GABA transporter 1 (hGAT1) in *X. laevis* oocytes and used electrophysiological measurements to determine Q_{max} and I_{max} as well as used freeze-fracture and electron microscopy to determine GAT1 density in the plasma membrane of the same cells in which functional data were collected. Transporter density in the plasma membrane and whole-cell capacitance measurements from the same cells allowed estimation of the total number of transporters giving rise to the macroscopic signal. At 21°C and −50 mV, the GAT1 turnover rate was estimated to be 15 ± 2 s^{-1}. When extrapolated to

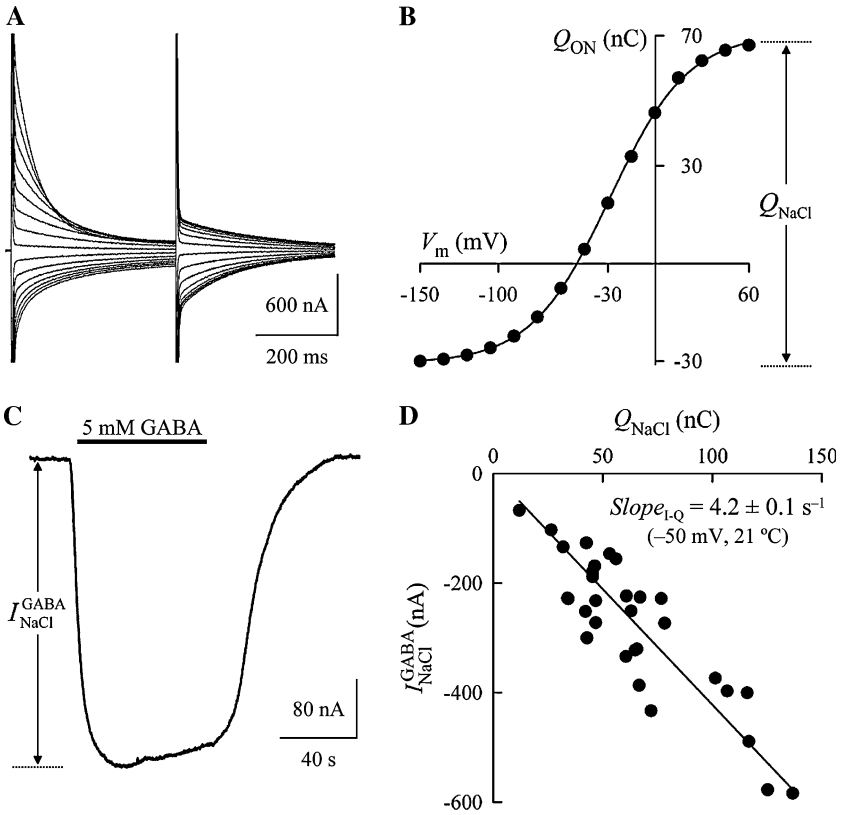

Fig. 1 The GABA-evoked current (I^{GABA}_{NaCl}) is directly related to the voltage-activated transporter charge movements (Q_{NaCl}). **a** An oocyte expressing GAT1 was subjected to a series of 400-ms voltage pulses ranging from +60 to –150 m*V* (in 15-m*V* steps), and the resulting current traces were recorded. The holding voltage was –50 m*V*, $[Na^+]_o$ was 100 mM and $[Cl^-]_o$ was 106 mM. **b** At each test voltage, the hGAT1 pre-steady-state current transients were isolated from oocyte capacitive and steady-state leak currents. The time integral of the pre-steady-state currents for the ON response then yielded the charge-voltage (*Q-V*) relationship. Fit of the *Q-V* relationship with a single Boltzmann function (equation 3) yielded the following parameters: Q_{NaCl}, 101 nC; $V_{0.5}$, –29 m*V*; and $z\delta$, 1.0. **c** Following Q_{NaCl} measurement (**b**), the same cell was exposed to a saturating GABA concentration (5 mM), and the GABA-evoked current (I^{GABA}_{NaCl}) was recorded (V_m = –50 mV). **d** Q_{NaCl} and I^{GABA}_{NaCl} (at –50 m*V*) were measured in a group of hGAT1-expressing oocytes (as shown in **a–c**). We refer to this plot as the *I–Q* relationship. Each data point corresponds to Q_{NaCl} and I^{GABA}_{NaCl} measurements from a single GAT1-expressing oocyte. A linear regression through the data points yielded a slope ($Slope_{I-Q}$) of 4.2 ± 0.1 s^{-1} (n = 31). The measurements were obtained at 21 ± 1°C. $Slope_{I-Q}$ was voltage-dependent (see Table 1)

physiological temperature (37°C) and membrane potentials (−50 to −90 m*V*), the GAT1 turnover rate was estimated to be 79–93 s^{-1}. These results suggest that previous measurements underestimated the turnover rate and, moreover, that the turnover rate is sufficient to bring about rapid GABA clearance at fast GABAergic synapses.

Materials and Methods

Expression in *Xenopus* Oocytes

Stage V–VI *X. laevis* oocytes were injected with 50 ng of cRNA for hGAT1 (SLC6A1) (Nelson, Mandiyan & Nelson, 1990; Chen, Reith & Quick, 2004). After cRNA injection, oocytes were maintained in Barth's medium (in mM: 88 NaCl, 1 KCl, 0.33 $Ca[NO_3]_2$, 0.41 $CaCl_2$, 0.82 $MgSO_4$, 2.4 $NaHCO_3$, 10 4-[2-hydroxyethyl]-1-piperazineethanesulfonic acid [HEPES, pH 7.4], as well as 50 μg/ml gentamicin, 100 μg/ml streptomycin and 100 units/ml penicillin) at 18°C for up to 14 days until used in experiments. Unless otherwise indicated, experiments were performed at 21 ± 1°C.

Experimental Solutions and Reagents

Unless otherwise indicated, experiments were performed in a NaCl buffer containing (in mM) 100 NaCl, 2 KCl, 1 $CaCl_2$, 1 $MgCl_2$ and 10 HEPES (pH 7.4). In Na^+-free solutions, NaCl was isosmotically replaced with choline-Cl. In Cl^--free solutions, NaCl, KCl, $CaCl_2$ and $MgCl_2$ were isosmotically replaced with corresponding gluconate salts. Choline and gluconate do not interact with the GATs

(Mager et al., 1993; Sacher et al., 2002; Karakossian et al., 2005). GABA was added to the above solutions as indicated. In experiments in which high (>1 mM) GABA concentrations were used, the osmolarity of corresponding control solutions was adjusted by isosmotic addition of mannitol. [^{3}H]-GABA was obtained from GE Healthcare (Piscataway, NJ). Glutaraldehyde, amyl acetate and collodion were obtained from Electron Microscopy Sciences (Hatfield, PA). All other reagents were purchased from Fisher Scientific (Pittsburgh, PA) or Sigma (St. Louis, MO).

Electrophysiological Measurements and Data Analysis

The two-microelectrode voltage-clamp technique was used for recording of whole-cell transporter-mediated currents. Oocytes were voltage-clamped using the Warner Oocyte Clamp (OC-725C; Warner Instrument, Hamden, CT). In the experimental recording chamber, oocytes were initially stabilized in the NaCl buffer, and the composition of the bath was changed as indicated. In all experiments, the reference electrodes were connected to the experimental oocyte chamber via agar bridges (3% agar in 3 M KCl). For continuous holding current measurements, currents were low pass-filtered at 1 Hz (LPF 8, Warner Instrument) and sampled at 10 Hz (pCLAMP 8.1; Axon Instruments, Union City, CA). Experimental temperature variations were achieved using a Warner Instrument TC-324B Automatic Temperature Controller and an in-line solution heater (SH-27B), as described previously (Karakossian et al., 2005).

Substrate-induced steady-state cotransporter currents were obtained as the difference between the steady-state currents in the absence and presence of GABA. The effects of substrate concentration ($[GABA]_o$, $[Na^+]_o$ and $[Cl^-]_o$) on the steady-state kinetics were determined by nonlinear curve fitting of the induced currents (I) with equation 1:

$$I = \frac{I^S_{\max} \cdot [S]^n}{(K^S_{0.5})^n + [S]^n} \tag{1}$$

where S is the substrate (GABA, Na^+ or Cl^-), $I^S_{\max}$ is the maximal substrate-induced current, $K^S_{0.5}$ is the substrate concentration at half $I^S_{\max}$ (half-maximal concentration) and n is the Hill coefficient. For kinetic characterization of Cl^- activation of the inward currents, an additional linear term was added to equation 1 in order to account for the non-zero baseline at zero Cl^- concentration (*see* Fig. 3e). As the GABA-evoked current is Na^+- and Cl^--coupled (Loo et al., 2000), it is henceforth referred to as I^{GABA}_{NaCl}. For steady-state current-voltage (I-V) relations, the pulse protocol (pCLAMP 8.1) consisted of 400-ms voltage steps from a holding potential of −50 mV to a series of test voltages (V_m) from +60 to −150 mV in 15-mV steps. Currents were low pass-filtered at 500 Hz and sampled at 2 kHz. At each voltage, the steady-state GABA-evoked current was obtained as the difference in steady-state current in the absence and presence of GABA.

To examine the carrier-mediated pre-steady-state current transients, the pulse protocol consisted of voltage jumps (400 ms) from the holding voltage (−50 mV) to test voltages ranging from +60 to −150 mV in 15-mV steps. Unless otherwise indicated, voltage pulses were separated by an interval of at least 3 s in order to allow for complete relaxation of the OFF transients (*see* Sacher et al., 2002; Karakossian et al., 2005). Currents were low pass-filtered at 1 kHz and sampled at 12.5 kHz without averaging. To obtain the transporter pre-steady-state currents, at each V_m, the total current for the ON transients, $I(t)$, was fitted with equation 2:

$$I(t) = I_1 e^{-t/\tau_1} + I_2 e^{-t/\tau_2} + I_{SS} \tag{2}$$

where t is time, $I_1 e^{-t/\tau_1}$ is the oocyte capacitive transient current with initial value I_1 and time constant τ_1, $I_2 e^{-t/\tau_2}$ is the transporter transient current with initial value I_2 and time constant τ_2 and I_{ss} is the steady-state current (Loo et al., 1993; Hazama, Loo & Wright, 1997). At each V_m, the total transporter-mediated charge (Q) was obtained by integration of the transporter transient currents. The charge-voltage (Q-V) relations obtained were then fitted with a single Boltzmann function (equation 3):

$$\frac{Q - Q_{hyp}}{Q_{NaCl}} = \frac{1}{1 + e^{\left[\frac{-z\delta F(V_m - V_{0.5})}{RT}\right]}} \tag{3}$$

where $Q_{NaCl} = Q_{dep} - Q_{hyp}$ (Q_{dep} and Q_{hyp} are Q at depolarizing and hyperpolarizing limits, respectively) and represents the maximum charge moved (i.e., Q_{max}), z is the apparent valence of movable charge, δ is the fraction of the membrane electric field traversed by the charge, $V_{0.5}$ is the V_m for 50% charge movement, F is Faraday's constant, R is the gas constant and T is the absolute temperature.

To determine the total surface area of the plasma membrane of the cells that were used in freeze-fracture and electron microscopy studies, whole-cell membrane capacitance measurements were made under conditions which eliminate the transporter pre-steady-state charge movements. Control cells, which do not exhibit transporter pre-steady-state currents, were maintained at −50 mV, and 5-mV depolarizing pulses (10 ms) were applied. For hGAT1-expressing oocytes, from a holding potential of −50 mV, the membrane was prepulsed to −5 mV for 1 s, and a 5-mV depolarizing pulse (10 ms) was applied. The measurements were carried out in the absence of external Na^+ (choline replacement) in order to eliminate transporter charge movements at the voltage tested (Mager

et al., 1993). Currents were low pass-filtered at 5 kHz and sampled at 10 kHz. After subtraction of the steady-state currents, whole-cell capacitance was determined from the time integral of the oocyte capacitive transients ($C_m = q/V_t$, where C_m is the membrane capacitance, q is the charge obtained from the integral of the capacitive transient current and V_t is the test voltage amplitude of 5 m*V*) and is reported as the average of values obtained from the ON and OFF transients. The choice of the prepulse potential (−5 m*V*) was based on the GAT1 *Q-V* relationship in the absence of external Na^+ as at this voltage and absence of external Na^+ no carrier-mediated charge movement is present (*not shown; see* Mager et al., 1993, for rat GAT1). The total surface area of the plasma membrane was determined using the whole-cell capacitance and a specific membrane capacitance of 1 μF/cm^2 (Zampighi et al., 1995; Hirsch, Loo & Wright, 1996; Forster et al., 1999; Zhang & Hamill, 2000). Under the conditions described above, capacitance measurements were also performed in the presence of the specific GAT1 inhibitor NO-711 (20 μM), and the results were similar to those in the absence of inhibitor (*not shown*).

To determine the relationship between the GABA-evoked current and GABA uptake, uptake experiments were performed under voltage clamp (Eskandari et al., 1997; Loo et al., 2000; Sacher et al., 2002; Whitlow et al., 2003; Karakossian et al., 2005). The membrane potential was held at the indicated value (−10, −50 or −90 m*V*), and the holding current was continuously monitored. Oocytes were initially incubated in the NaCl buffer until baseline was established. GABA (25 or 500 μM) and [^{3}H]-GABA (30 nM) were added to the perfusion solution for 5–10 min. At the end of the incubation period, GABA and the isotope were removed from the perfusion solution until the holding current returned to the baseline. The oocytes were removed from the experimental chamber, washed in ice-cold choline-Cl buffer and solubilized in 10% sodium dodecyl sulfate. Oocyte [^{3}H]-GABA content was determined in a liquid scintillation counter (LS 6500; Beckman, Fullerton, CA). Net inward charge was obtained from the time integral of the GABA-evoked inward current and correlated with GABA influx in the same cell. To examine the effect of temperature, experiments looking at uptake under voltage clamp were performed at 21°C and 32°C.

Pre-steady-state and steady-state curve fittings were performed using either SigmaPlot (SPSS Science, Chicago, IL) or software developed in this laboratory. Where sample sizes are indicated (*n*), they refer to the number of oocytes in which the experiments were repeated. Reported errors represent the standard error (SE) of the mean obtained from data on several oocytes.

Freeze-Fracture and Electron Microscopy

A major aim of this study was to measure and correlate the macroscopic rate of GABA transport and the total number of GABA transporters in the plasma membrane of individual cells expressing GAT1. Two parameters may be used as the macroscopic measure of transporter function, I_{NaCl}^{GABA} and Q_{NaCl}, both of which are related to the total number of functional transporters in the plasma membrane (Zampighi et al., 1995; Eskandari et al., 2000). Here, we measured Q_{NaCl} as the macroscopic assay of GAT1 function in cells used for freeze-fracture and electron microscopy. Q_{NaCl} is obtained in the absence of GABA (*see* Fig. 1a) and is directly proportional to I_{NaCl}^{GABA} (*see* Fig. 1d) (Mager et al., 1993; Fesce et al., 2002; Sacher et al., 2002; Karakossian et al., 2005).

In a group of oocytes, both Q_{NaCl} and whole-cell capacitance (C_m) were measured (*see above*). The same cells were then prepared for freeze-fracture and electron microscopy (Chandy et al., 1997; Eskandari et al., 1997, 1998, 1999, 2000; Zampighi et al., 1995, 1999). Following Q_{NaCl} and C_m measurements, oocytes were immediately fixed for 1 h in 3% glutaraldehyde in 0.1 M sodium cacodylate (pH 7.35). In preparation for freeze-fracture, fixed oocytes were cryoprotected for 1 h with 25% glycerol in 0.1 M sodium cacodylate. Each oocyte was then cut into three or four pieces, and each piece was placed on a gold specimen holder, rapidly frozen by immersion in liquid propane and stored in a liquid nitrogen freezer. In most experiments, one frozen sample of a given oocyte was randomly selected for freeze-fracture analysis (i.e., no preference was given to animal or vegetal pole fragments). In a few experiments, two or more samples of the same oocyte (corresponding to different plasma membrane regions of the same cell) were examined to study the regional distribution of GAT1 on the cell surface (*see* "Results"). Frozen samples were fractured in a JEOL/RMC RFD-9010CR freeze-fracture-etch apparatus (Boeckeler Instruments, Tucson, AZ) at −120°C and $\leq 2.2 \times 10^{-5}$ Pa. The fracture faces were replicated with platinum-carbon (Pt-C) at 80°, and the replica was stabilized by carbon deposition at 90° (both at −120°C). Replicas were cleaned in sodium hypochlorite, washed in ultrapure water and placed on 100-mesh carbon/formvar-coated copper grids.

Replicas were examined in a Zeiss (Thornwood, NY) 10C transmission electron microscope at 80 k*V*. Electron images were recorded on Kodak (Rochester, NY) SO-163 electron image film at 25,000× to 100,000×. The electron films were digitized at 1,200 dpi, giving rise to a final pixel size of 0.21–0.84 nm. Data analyses of particle density and size were carried out using ImageJ (National Institutes of

Health, Bethesda, MD) as described previously (Eskandari et al., 1998, 2000).

Twenty-two replicas from 18 hGAT-1-expressing oocytes and 10 replicas from 10 control oocytes were examined for this study. In each replica, several P (protoplasmic) face regions of the plasma membrane were identified. For each P face region, the area as well as the number of intramembrane particles present in that area were determined. A plot of the number of particles found in a given region as a function of the region area yielded a linear relationship. Using a simple linear regression, the slope of this plot was taken as the P face particle density for the oocyte. The density and the total cell surface area (obtained from whole-cell capacitance; *see above*) were then used to estimate the total number of P face intramembrane particles in the plasma membrane of the oocyte. Control cells were subjected to the same analysis in order to estimate the number of endogenous P face integral membrane proteins.

Results

Correlation between the GABA-Evoked Current (I_{NaCl}^{GABA}) and Voltage-Activated Transporter Charge Movements (Q_{NaCl})

Figure 1 demonstrates the conventional approach for estimating the turnover rate of electrogenic Na^+-coupled transporters. The correlation between the GABA-evoked current (I_{NaCl}^{GABA}) and the voltage-induced transporter charge movements (Q_{NaCl}) was examined in a group of GAT1-expressing oocytes (Fig. 1). In each cell, Q_{NaCl} was measured in the absence of GABA (Fig. 1a, b) and, subsequently, I_{NaCl}^{GABA} was measured at a saturating GABA concentration (all at 21°C) (Fig. 1c). I_{NaCl}^{GABA} was voltage-dependent (*see* Fig. 2c), whereas Q_{NaCl} did not depend on the holding potential. I_{NaCl}^{GABA} plotted as a function of Q_{NaCl} (*I-Q* relationship) revealed a linear correlation with a slope ($Slope_{I\text{-}Q}$) of $4.2 \pm 0.1\ s^{-1}$ (at -50 m*V* and 21°C) ($n = 31$) (Fig. 1d, Table 1). Although it is commonly accepted that the slope of the *I-Q* relationship yields the transporter turnover rate (Loo et al., 1993; Mager et al., 1993; Fesce et al., 2002; Sacher et al., 2002; Karakossian et al., 2005), we provide evidence in this study that this slope underestimates the GAT1 turnover rate.

Temperature and Voltage Dependence of GAT1 Charge Flux:GABA Flux Ratio

Figure 2a shows GAT1 GABA-evoked (1 mM) responses at 21°C (left trace) and 31°C (right trace). At 31°C, the GABA-evoked current was 280 ± 10% of that at 21°C ($n = 11$). The temperature coefficient (Q_{10}, 21–31°C) for the GABA-evoked steady-state current was 2.8 ± 0.1 for GAT1 ($n = 11$). When measured at -10 and -90 m*V*, Q_{10} was not significantly different from that measured at -50 m*V* (*not shown*), a result that has also been reported for other Na^+-coupled transporters (Parent & Wright, 1993; Bacconi et al., 2007). The Q_{10} (21–31°C) for the rat isoform of GAT1 (rGAT1) was 2.5 ± 0.1 ($n = 3$, *not shown*) and was slightly higher than the previously reported value of 2.2 for rGAT1 (Binda et al., 2002; Lu & Hilgemann, 1999a). Figure 2b shows an Arrhenius plot for the temperature dependence of I_{NaCl}^{GABA} (at -50 m*V* and 1 mM GABA). The activation energy (E_a), determined from the slope of a linear regression through the data points, was 20 ± 1 kcal/mol (Fig. 2b) ($n = 11$). The linear slope observed in the Arrhenius plot suggests that, in the temperature range tested (19–32°C), the rate-limiting step is the same in the transport cycle (Gutfreund, 1995; Segel, 1975). The GABA-evoked current increased with hyperpolarization and approached zero at depolarized potentials without reversing (Fig. 2c) (Mager et al., 1993; Loo et al., 2000; Fesce et al., 2002).

We then performed uptake experiments under voltage clamp at different temperatures, membrane voltages and GABA concentrations (Fig. 2d–f). This allowed us to examine the effect of temperature, membrane voltage and GABA concentration on the ratio of GAT1-mediated charge flux to GABA flux; i.e., the number of charges translocated across the plasma membrane per GABA molecule (*m*; see "Introduction" and "Discussion"). Although the GABA-evoked macroscopic current depended on temperature (Fig. 2a, b), membrane potential (Fig. 2c) and GABA concentration (*see* Fig. 3a), the ratio of charge flux to GABA flux was 2.0 ± 0.1 inward charges per GABA molecule translocated across the plasma membrane for all experimental conditions tested (Fig. 2e, f) ($n = 38$). Thus, in the temperature range (21–32°C), membrane potential range (-90 to -10 m*V*) and GABA concentration range (25–500 μM) tested, the number of charges translocated across the plasma membrane per GABA molecule appeared to be constant (Fig. 2e, f). The results demonstrate tight coupling between charge flux and GABA flux and, therefore, strongly argue against GAT1-mediated uncoupled currents (Cammack, Rakhilin & Schwartz, 1994; Krause & Schwarz, 2005).

Temperature and Voltage Dependence of Steady-State Kinetic Parameters of GAT1

We examined the effect of temperature on GAT1 apparent affinity for Na^+, Cl^- and GABA. The results suggest that the half-maximal concentration values for Na^+, Cl^- and GABA were not temperature-dependent (Fig. 3). Table 1

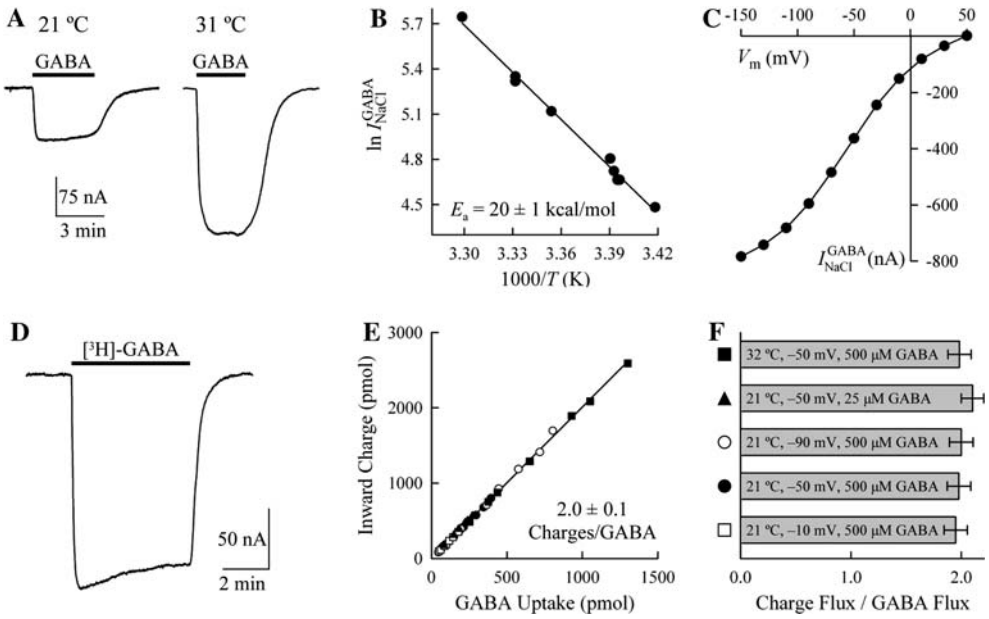

Fig. 2 Temperature and voltage dependence of GAT1 macroscopic and microscopic properties. **a** Steady-state GABA-evoked current traces were recorded at 21°C (*left trace*) and 31°C (*right trace*) from an oocyte expressing hGAT1 ($[Na^+]_o$ = 100 mM, $[Cl^-]_o$ = 106 mM, [GABA] = 1 mM, V_m = –50 m*V*). The GABA-evoked current increased 2.8-fold when the temperature was raised by 10°C. Q_{10} (21–31°C) for hGAT1 was 2.8 ± 0.1 (n = 11). Q_{10} was not voltage-dependent (*not shown*). **b** Arrhenius plot for the temperature dependence of I_{NaCl}^{GABA} yielded a linear relationship in the temperature range 19–32°C. Measurements were obtained at V_m = –50 m*V*. The *smooth line* is a linear regression through the data points. The activation energy (E_a) determined from the slope of the plot (E_a = – slope × R, where R is the gas constant) was 20 ± 1 kcal/mol (n = 11). **c** I_{NaCl}^{GABA} was also voltage-dependent. **d** GABA uptake experiments were performed under voltage clamp at different temperatures (21°C and 32°C), membrane potentials (–10, –50 and –90 m*V*) and GABA concentrations (25 and 500 µM). See "Materials and Methods" for details. **e, f** Net inward charge *vs.* GABA uptake in individual GAT1-expressing cells. Experiments were carried out under five different conditions, which examined the effect of temperature, membrane potential and GABA concentration on the charge/flux ratio; i.e., number of charges translocated per transport cycle (m in equations 4, 6, 7). Three experiments were carried out at 21°C and 500 µM GABA and examined the effect of membrane voltage at –10 m*V* (1.9 ± 0.1 charges/GABA, *open squares*, n = 7), –50 m*V* (2.0 ± 0.1 charges/GABA, *filled circles*, n = 10) and –90 m*V* (2.0 ± 0.1 charges/GABA, *open circles*, n = 8). The fourth experiment was performed at 21°C and –50 m*V* and examined the effect of a subsaturating GABA concentration (25 µM) on the charge/flux ratio (2.1 ± 0.1 charges/GABA, *filled triangles*, n = 6). The fifth experiment examined the effect of temperature and was performed at 32°C, –50 m*V* and 500 µM GABA (2.0 ± 0.1 charges/GABA, *filled squares*, n = 7). In all experiments, $[Na^+]$ = 100 mM and $[Cl^-]$ = 106 mM. The *smooth line* represents a linear regression through all data points with a slope of 2.0 ± 0.1 charges per GABA (n = 38). The ratio of inward charge to GABA uptake was independent of temperature, GABA concentration and membrane potential (**f**). At 21°C, endogenous uptake of GABA in control cells was not voltage-dependent (0.14 ± 0.03 pmol/min/oocyte); however, it did increase at 32°C (0.79 ± 0.14 pmol/min/oocyte). To determine GAT1-mediated GABA uptake, endogenous GABA uptake was subtracted from total uptake in GAT1-expressing cells. In GAT1-expressing cells, uptake rates ranged 15–465 pmol/min/oocyte

presents the half-maximal concentration values (i.e., apparent affinity constants) for GABA, Na^+ and Cl^- in the limited voltage range of −90 to −10 m*V*. While the apparent affinity for Na^+ and Cl^- increased with hyperpolarization, the apparent affinity for GABA decreased with hyperpolarization (Kavanaugh et al., 1992; Mager et al., 1993; Forlani et al., 2001a; Fesce et al., 2002). Despite numerous attempts, we did not succeed in obtaining reliable Na^+ or Cl^- kinetic data sets at higher NaCl concentrations as oocytes became increasingly unstable upon prolonged exposure to solutions of higher osmolarity (*not shown*). However, we were able to obtain data from short exposures of oocytes to solutions in which the Na^+ and/or Cl^- was increased to 150 mM (*see below* and Fig. 4).

The above kinetics data suggest that at standard Na^+ (100 mM) and Cl^- (106 mM) concentrations used in the bathing medium of *X. laevis* oocytes, the GAT1 GABA-evoked current (I_{NaCl}^{GABA}) does not represent the maximum macroscopic current (i.e., I_{max}) (*see also* Bicho & Grewer, 2005). Thus, we examined whether a supersaturating GABA concentration could drive transport to its maximum velocity (even at subsaturating Na^+ and Cl^- concentrations), as would be predicted by an ordered kinetic scheme in which GABA is the last cosubstrate to bind to the transporter from the extracellular side (*see* Parent et al., 1992; Eskandari et al., 1997; Hilgemann & Lu, 1999; Forster et al., 2002; Sacher et al., 2002; Whitlow et al., 2003; Karakossian et al., 2005). The results are summarized in Figure 4. At 100 mM Na^+ and 106 mM Cl^-, I_{NaCl}^{GABA}

Table 1 Summary of GAT1 turnover rate data

V_m (mV)	$K_{0.5}^{Na}$ (mM)[a]	$K_{0.5}^{Cl}$ (mM)[a]	$K_{0.5}^{GABA}$ (μM)[a]	f_I [b]	$Slope_{I\text{-}Q}$ at 21°C(s^{-1})[c]	$Slope_{I\text{-}Q}$ at 37°C (s^{-1})[c]	R_T at 21°C (s^{-1})[d]	R_T at 37°C (s^{-1})[d]
−10	108 ± 17	88 ± 21	17 ± 6	0.31 ± 0.07	0.9 ± 0.1	4.4 ± 0.1	6 ± 1	29 ± 5
−30	88 ± 15	81 ± 21	22 ± 6	0.39 ± 0.09	2.5 ± 0.1	13.1 ± 0.1	13 ± 2	67 ± 11
−50	65 ± 5	47 ± 5	26 ± 4	0.55 ± 0.05	4.2 ± 0.1	21.8 ± 0.1	15 ± 2	79 ± 11
−70	53 ± 6	27 ± 8	30 ± 9	0.67 ± 0.09	5.9 ± 0.1	30.5 ± 0.1	18 ± 3	92 ± 13
−90	33 ± 4	9 ± 3	34 ± 7	0.85 ± 0.09	7.6 ± 0.1	39.3 ± 0.1	18 ± 3	93 ± 13

[a] The half-maximal concentration values ($K_{0.5}^{Na}$, $K_{0.5}^{Cl}$ and $K_{0.5}^{GABA}$) were determined experimentally at the indicated voltages (*see* Fig. 3 for experiments at –50 mV). GABA kinetics experiments were performed at 100 mM Na^+ and 106 mM Cl^-. Sodium kinetics experiments were performed at 106 mM Cl^- and 5 mM GABA. Chloride kinetics experiments were performed at 100 mM Na^+ and 5 mM GABA. The values represent the mean ± SE from four or more oocytes. $K_{0.5}$ values obtained at 21°C and 31°C were similar

[b] f_I values were calculated according to equation 5 using the corresponding half-maximal concentrations

[c] $Slope_{I\text{-}Q}$ values were obtained experimentally at 21°C and at the indicated voltages (*see* Fig. 1d for experiments at –50 mV). The temperature dependence of I_{NaCl}^{GABA} (equation 8, Q_{10} = 2.8 ± 0.1) was used to estimate the values of $Slope_{I\text{-}Q}$ at 37°C. Q_{10} was not voltage-dependent.

[d] R_T values at 21°C and 37°C were calculated according to equation 7 using the corresponding $Slope_{I\text{-}Q}$ values. m was experimentally measured at –90 (2.0 ± 0.1), –50 (2.0 ± 0.1) and –10 (1.9 ± 0.1) mV (Fig 2d–f). Thus, we used m = 2.0 ± 0.1 to calculate R_T at –70 and –30 mV. $z\delta$ (4 ± 1) was obtained from the experiments of Figures 5–8. m and $z\delta$ were neither temperature- nor voltage-dependent

increased only slightly as the GABA concentration was increased from 1 to 20 mM (Fig. 4). The increase in I_{NaCl}^{GABA} was consistent with a dependence on GABA concentration, with a $K_{0.5}$ of ~25 μM. I_{NaCl}^{GABA} was larger when the Na^+ or Cl^- concentration was increased to 150 mM and even larger when both Na^+ and Cl^- concentrations were increased to 150 mM (Fig. 4). Thus, at the usual extracellular Na^+ (100 mM) and Cl^- (106 mM) concentrations used for *X. laevis* oocyte experiments, the GABA-evoked current does not represent the maximum current (I_{max}) mediated by GAT1 (see "Discussion").

Examination of GAT1 in the Plasma Membrane by Freeze-Fracture and Electron Microscopy

The electrophysiological estimate of the transporter turnover rate (e.g., Fig. 1d) suffers from a lack of ability to determine the total number of functional transporters in the plasma membrane. Although the charge moved (Q_{NaCl}) is directly related to the total number of functional transporters in the plasma membrane (Zampighi et al., 1995; Chandy et al., 1997; Eskandari et al., 2000), the number of transporters obtained from Q_{NaCl} relies on the electrophysiological estimate of $z\delta$, as determined from a fit of the charge-voltage relationship with a single Boltzmann function (*see* Fig. 1b and equation 3) (Loo et al., 1993; Mager et al., 1993; Wang et al., 2003; Bicho & Grewer, 2005). Many electrogenic Na^+-coupled transporters exhibit a value of unity for $z\delta$, although values lower and higher than unity have also been reported (Loo et al., 1993; Mager et al., 1993; Wadiche et al., 1995; Eskandari et al., 1997; Hazama et al., 1997; Lu & Hilgemann, 1999b; Forster et al., 2002; Sacher et al., 2002; Karakossian et al., 2005). For GAT1, $z\delta$ is ~1 (Mager et al., 1993, 1996; Loo et al., 2000; Forlani et al., 2001a; Whitlow et al., 2003). For the closely related GAT3 and GAT4, $z\delta$ values are 1.6 and 1.8, respectively (Sacher et al., 2002; Whitlow et al., 2003; Karakossian et al., 2005).

As the electrophysiological estimate of the total number of transporters may or may not be valid (*see* Zampighi et al., 1995), we elected to combine electrical measurements with freeze-fracture and electron microscopic examination of the oocyte plasma membrane in order to provide an estimate of the total number of transporters in the plasma membrane (Figs. 5–8). For these measurements, Q_{NaCl} and whole-cell capacitance were measured, and the same cells were processed for analysis by freeze-fracture and electron microscopy. Whole-cell capacitance was combined with electron microscopic determination of transporter density in the plasma membrane in order to estimate the total number of transporters at the cell surface. The correlation between Q_{NaCl} and the total number of transporters then yielded the value of $z\delta$ (*see* Fig. 7).

Figure 5 shows representative freeze-fracture images from a control cell (Fig. 5a) and two hGAT1-expressing oocytes exhibiting different levels of GAT1 expression in the plasma membrane (Fig. 5b, c). In control cells, the density of endogenous particles was 298 ± 20/μm^2 (n = 6 oocytes) (*see also* Eskandari et al., 1998; Bron et al., 1999), and the endogenous density appeared to be independent of the time of measurement after extraction from the donor frog (*see* Fig. 6b). In cells expressing GAT1, the density of P face particles was directly related to Q_{NaCl} (Fig. 5b, c; *see also* Fig. 7). For example, in the cell shown in Figure 5b, Q_{NaCl} was 44 nC and the density of P face particles

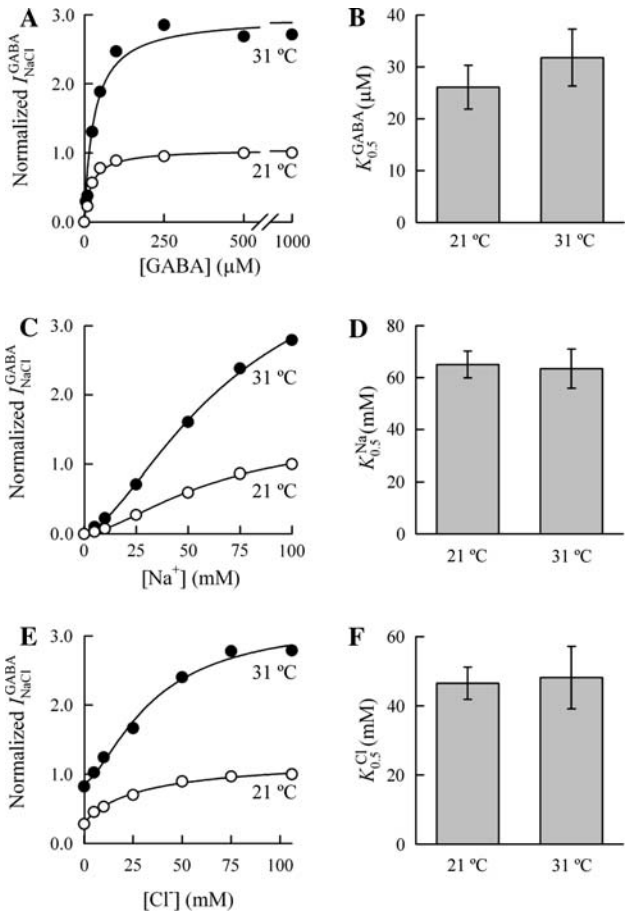

Fig. 3 Apparent affinities for Na^+, Cl^- and GABA are not temperature-dependent. **a** Representative kinetic curves are shown at 21°C (*open circles*) and 31°C (*filled circles*) for the evoked currents as a function of GABA concentration. $[Na^+]_o$ = 100 mM, $[Cl^-]_o$ = 106 mM. **b** The half-maximal concentration for GABA ($K_{0.5}^{GABA}$) was the same at the two temperatures examined; $K_{0.5}^{GABA}$ was 26 ± 4 μM at 21°C (n = 16) and 32 ± 5 μM at 31°C (n = 4). **c** Representative Na^+ kinetics experiments are shown at 21°C and 31°C. Both data sets were obtained from the same hGAT1-expressing oocyte. The increase in temperature did not alter the half-maximal Na^+ concentration ($K_{0.5}^{Na}$) or the Hill coefficient for Na^+ activation of the inward currents. The Hill coefficient for Na^+ activation of the inward currents was 1.5 ± 0.1 at both 21°C (n = 11) and 31°C (n = 4). $[GABA]_o$ = 5 mM, $[Cl^-]_o$ = 106 mM. **d** $K_{0.5}^{Na}$ was 65 ± 5 mM at 21°C (n = 11) and 63 ± 8 mM at 31°C (n = 4). **e** Representative Cl^- kinetics experiments are shown at 21°C and 31°C. The increase in temperature did not alter the half-maximal concentration for Cl^- ($K_{0.5}^{Cl}$), but it increased the Hill coefficient for Cl^- activation of the inward current as the dose-response curve assumed a sigmoidal relationship at 31°C. The Hill coefficient for Cl^- activation of the inward currents was 0.9 ± 0.1 (n = 11) at 21°C and 1.6 ± 0.1 (n = 4) at 31°C. The difference between the two Hill coefficients was statistically significant (Student's t-test $p = 1.3 \times 10^{-5}$). $[Na^+]_o$ = 100 mM, $[GABA]_o$ = 5 mM. **f** $K_{0.5}^{Cl}$ was 47 ± 5 mM at 21°C (n = 11) and 48 ± 9 mM at 31°C (n = 4). The kinetic curves in **a, c** and **e** were normalized to the maximal substrate-induced current at 21°C, and the *smooth line* is a fit of the data to equation 1. The reported values are for V_m = −50 mV (*see* Table 1 for values at other voltages). In **e**, an additional linear term was added to account for the non-zero baseline at zero Cl^- concentration. The data shown in **b, d** and **f** represent the mean ± SE from four oocytes

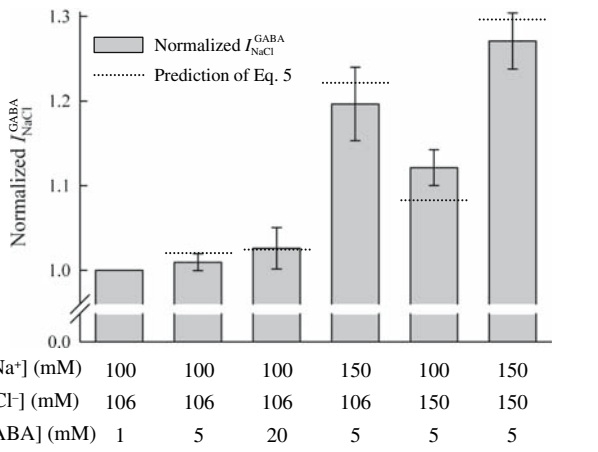

Fig. 4 Dependence of GAT1-mediated macroscopic current (I_{NaCl}^{GABA}) on the external concentrations of Na^+, Cl^- and GABA. The current mediated by GAT1 was examined at the indicated external concentrations of Na^+, Cl^- and GABA (in mM). V_m = –50 mV. For each concentration, the evoked current was normalized to that obtained at 100 mM Na^+, 106 mM Cl^- and 1 mM GABA in the same cell. For each experimental condition, the reported value is the mean ± SE from five or more oocytes. To control for osmotic changes brought about by addition of GABA, equimolar amounts of mannitol were added to the corresponding control solutions. The experimental data (*gray bars*) were in reasonable agreement with the predicted dependence of I_{NaCl}^{GABA} on the Na^+, Cl^- and GABA concentrations (*dotted lines*, as predicted by equation 5; *see* "Discussion")

increased to 1,190 ± 35/μm^2. The whole-cell capacitance (C_m) in this cell was 321 nF. In Figure 5c, Q_{NaCl} was 187 nC and the corresponding P face particle density was 3,739 ± 98/μm^2 (C_m = 583 nF). In the same fashion, we examined the relationship between Q_{NaCl} and the total number of P face particles in 10 oocytes exhibiting different levels of GAT1 expression (*see* Fig. 7).

Zampighi and colleagues (1995) showed that the intramembrane particles of membrane proteins heterologously expressed in oocytes partition only to the P face. We observed the same pattern with GAT1. The density of E (exoplasmic) face particles was the same in control oocytes (631 ± 34/μm^2) and GAT1-expressing cells (633 ± 84/μm^2, Q_{NaCl} range 34–114 nC). Therefore, our studies have focused on P face particles of control and GAT1-expressing cells.

We were interested in establishing that GAT1 expression was uniform over the entire surface of the cell. As described in "Materials and Methods," each cell was cut into three or four pieces. In most experiments, one oocyte fragment was randomly selected, replicated by freeze-fracture and examined under the electron microscope. In many oocytes, we were able to obtain data from two replicas (i.e., two distant plasma membrane regions of the same oocyte), and the density measurements obtained from different regions of the plasma membrane were not significantly different (*not shown*). Notably, in one GAT1-

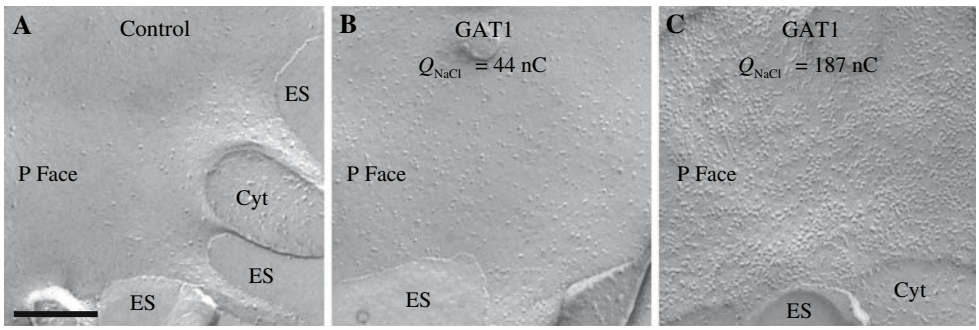

Fig. 5 Freeze-fracture micrographs of the plasma membrane of control and GAT1-expressing oocytes. **a** The P face of the plasma membrane of control oocytes contained 298 ± 20 particles/μm^2 (n = 6 oocytes). The density did not change significantly up to 10 days after cell isolation (*see* Fig. 6b). **b** In an oocyte in which Q_{NaCl} was 44 nC, the density of P face particles increased to 1,190 ± 35/μm^2. C_m was 321 nF in this cell. **c** The P face particle density increased to 3,739 ± 98/μm^2 in an oocyte in which Q_{NaCl} was 187 nC. C_m was 583 nF in this cell. Heterologous proteins expressed in oocytes do not partition to the E face (Zampighi et al., 1995). The density of E face particles was the same in control oocytes (631 ± 34/μm^2) and GAT1-expressing cells (633 ± 84/μm^2). Scale bar for **a**–**c** = 200 nm. *ES*, extracellular space; *Cyt*, cytoplasm; *P Face*, protoplasmic face

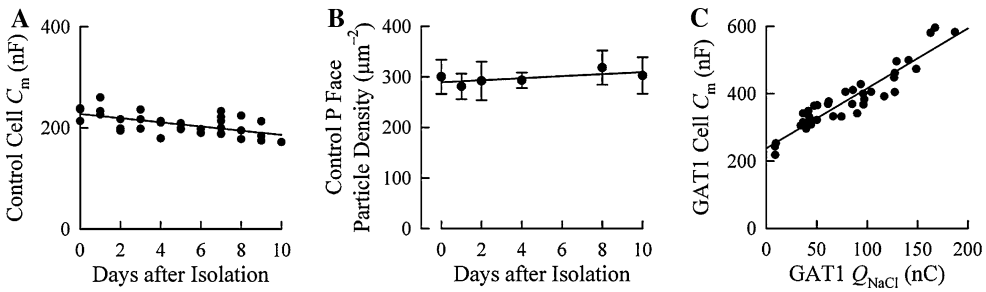

Fig. 6 Whole-cell capacitance (C_m) is used to estimate the total surface area of the cell plasma membrane. **a** Cells from the same batch were used to monitor C_m as a function of time after extraction from the donor frog (see "Materials and Methods"). In control cells, C_m decreased with a slope of –4 ± 1 nF/day (n = 3 batches of cells, where the batches contained 33, 44 and 49 cells). Thus, the total surface area of the plasma membrane in control cells decreases at a rate of ~400,000 μm^2/day. Baseline capacitance on day 0 (day of isolation from donor frog) was batch-dependent and ranged 213–322 nF. The average capacitance on day 0 was 260 ± 24 nF (n = 11). **b** The density of P face endogenous particles of control cells was 298 ± 20/μm^2 (n = 6 oocytes). No apparent trend of increase or decrease in the density was observed over the 10-day examination period. **c** In contrast to control cells, the C_m of GAT1-expressing cells increased directly with the level of GAT1 expression. The slope was 1.78 ± 0.11 nF/nC (n = 33). The predicted y-intercept at Q_{NaCl} = 0 is 238 ± 10 nF and is comparable to the C_m of control cells (**a**). Each data point represents C_m and Q_{NaCl} measurements from a single GAT1-expressing oocyte

expressing cell, we were able to obtain data from three replicas. The density measurements obtained from the three different plasma membrane regions (842 ± 86 μm^{-2}, 888 ± 76 μm^{-2} and 762 ± 185 μm^{-2}) were not significantly different (analysis of variance p = 0.072). Thus, GAT1 expression exhibited an even distribution in the oocyte plasma membrane.

In order to attribute the newly inserted intramembrane particles (such as those shown in Figure 5b, c) to the expression of GAT1 at the cell surface, we needed to characterize the endogenous P face particles (Fig. 6a, b). In a group of control cells, the whole-cell membrane capacitance was examined. The same cells were then fixed and prepared for freeze-fracture and electron microscopy in order to determine the density of P face freeze-fracture particles. When first isolated from the donor frog, the whole-cell membrane capacitance of stage V-VI *X. laevis* oocytes was 213–322 nF (Fig. 6a) (Isom et al., 1995; Hirsch et al., 1996). During the ensuing 10 days, whole-cell capacitance decreased at a rate of 4 ± 1 nF/day (n = 33), which is equivalent to a 1–2% reduction in the cell total surface area per day. Thus, the total surface area of the plasma membrane of control cells decreased with time at a rate of ~400,000 μm^2/day (using 1 μF/cm^2). Similar results were observed in three batches of oocytes. The rate of reduction in C_m was the same regardless of the initial magnitude of C_m. In some of the same cells in which C_m was measured, we also measured the density of P face intramembrane particles (Fig. 6b).

The density of endogenous particles in the P face did not change appreciably with time (Fig. 6b). The density was 298 ± 20/μm^2 (n = 6 oocytes), showing no significant change within 10 days of extraction from the donor frog. The observed pattern of whole-cell membrane capacitance

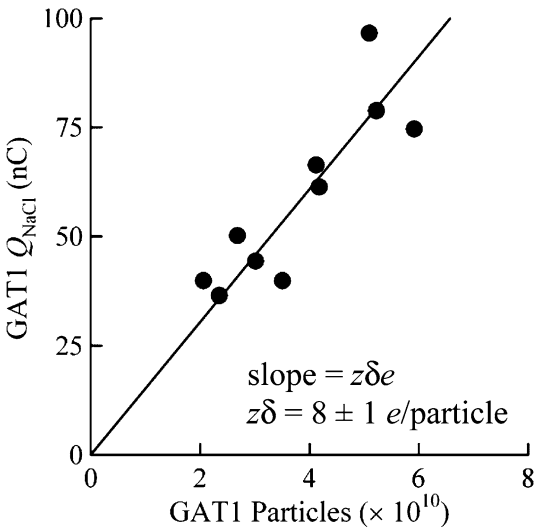

Fig. 7 Quantitative analysis of freeze-fracture images of GAT1 expression in the plasma membrane. In individual GAT1-expressing cells, Q_{NaCl} and whole-cell capacitance (C_m) were measured. The same cells were then fixed and examined by freeze-fracture and electron microscopy in order to determine the total number of GAT1 particles in the plasma membrane (*see* "Materials and Methods" and "Results"). The number of GAT1 particles in the plasma membrane was determined after correcting for the endogenous particles. GAT1 Q_{NaCl} was directly proportional to the total number of GAT1 particles in the plasma membrane. Q_{NaCl} is defined as $Q_{NaCl} = N_T z\delta e$. The slope (slope = $z\delta e$) of the linear regression through the data points was used to estimate the value of $z\delta$ to be 8 ± 1 elementary charges per GAT1 freeze-fracture particle (n = 10 oocytes). As the particles induced by GAT1 expression most likely represent GAT1 dimers (*see* Fig. 8 and "Discussion"), the apparent valence of GAT1 moveable charge is 4 ± 1 elementary charges per GAT1 monomer

and the density of P face particles in control cells were used to estimate the total number of endogenous P face particles. In GAT1-expressing cells, the total number of GAT1 particles in the plasma membrane was estimated after correcting for the endogenous particles.

Having examined the density of endogenous P face particles, we then focused on the P face particles of GAT1-expressing cells. In a group of GAT1-expressing cells, Q_{NaCl} and C_m were measured. The same cells were then processed for freeze-fracture and electron microscopy. Interestingly, in GAT1-expressing cells, C_m and, thus, the total surface area of the plasma membrane, increased directly with the level of GAT1 expression (Fig. 6c). Thus, it appears that fusion of GAT1-containing vesicles with the plasma membrane is not balanced by retrieval of the same amount of membrane. A similar observation was described for some membrane proteins expressed in *X. laevis* oocytes (Isom et al., 1995; Hirsch et al., 1996); however, an increase in plasma membrane area is not seen with all membrane proteins expressed in oocytes (Isom et al., 1995; Zampighi et al., 1999; Trotti et al., 2001). The increase in the measured C_m of GAT1-expressing cells was not due to GAT1-mediated capacitive charge movements because (1) the capacitance measurements were performed under conditions that eliminate GAT1 charge movements (see "Materials and Methods") and (2) under these conditions, C_m was the same in the absence and presence of the specific GAT1 inhibitor NO-711 (20 μM, n = 4; *not shown*).

Correlation between Q_{NaCl} and the Number of Transporters in the Plasma Membrane

When examined in the same cells, Q_{NaCl} was directly related to the total number of GAT1 particles in the plasma membrane (Fig. 7). Only GAT-expressing cells with Q_{NaCl} ≤ 100 nC were used in these experiments. At higher

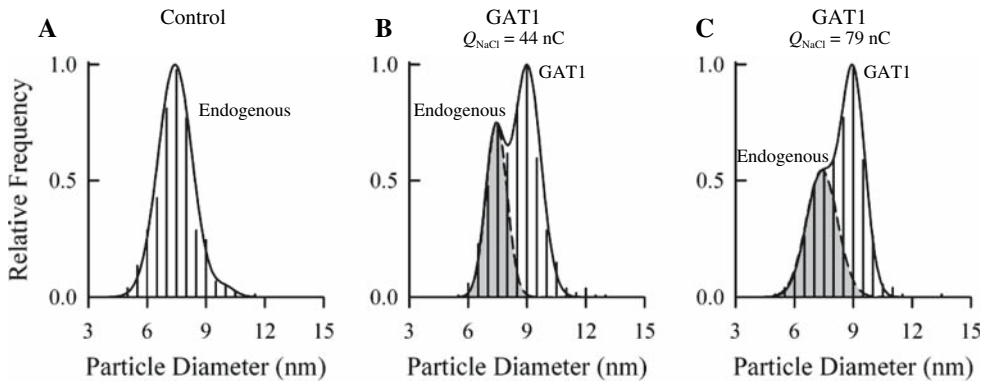

Fig. 8 Size frequency histograms of P face particles of control and GAT1-expressing cells. **a** In control cells, most of the endogenous particles have a mean diameter of 7.5 ± 0.6 nm (n = 462) (Eskandari et al., 1998). **b, c** Size frequency histogram of P face particles of GAT1-expressing cells revealed two prominent particle populations: one had a mean diameter of ~7.5 nm, corresponding to endogenous P face proteins (*shaded area*), and the second had a mean diameter of 9.0 ± 0.5 nm (n = 512 for **b** and n = 550 for **c**). The 9-nm particle population was present only in GAT1-expressing cells, and its relative frequency was proportional to the level of GAT1 expression. Q_{NaCl} was 44 nC in the oocyte of **b** and 79 nC in that of **c**. The cross-sectional area of the 9-nm freeze-fracture particle predicted an integral membrane protein complex composed of 24 ± 3 transmembrane α-helices (using 1.4 nm^2/helix; *see* Eskandari et al., 1998)

expression levels, overlapping freeze-fracture particle shadows did not allow us to obtain reliable density measurements (see Fig. 5c). Transporter density in the plasma membrane (obtained from freeze-fracture) and C_m in the same cell (obtained electrophysiologically) were used to determine the total number of transporters in the plasma membrane (after correction for the endogenous particles). Q_{NaCl} is related to the total number of functional transporters according to $Q_{NaCl} = N_T z\delta e$. The slope of the plot in Figure 7 was used to estimate the value of $z\delta$ to be 8 ± 1 elementary charges per GAT1 particle (using 1.602×10^{-19} C for e).

Thus far, the results suggest an apparent valence ($z\delta$) of 8 ± 1 elementary charges per GAT1 particle. However, it is possible that the GAT1 freeze-fracture particle is a complex of two or more GAT monomers. To examine the oligomeric state of GAT1 in the oocyte plasma membrane, we analyzed the size distribution of the P face particles of control and GAT1-expressing cells (Fig. 8). Most of the endogenous P face particles belong to a population of particles of 7.5 ± 0.6 nm diameter (Fig. 8a) (Eskandari et al., 1998). The 7.5-nm endogenous particles were also present in cells expressing GAT1 (Fig. 8b, c). Expression of GAT1 in oocytes led to the appearance of a new population of P face particles with a mean diameter of 9.0 ± 0.4 nm (Fig. 8b, c). The relative frequency of the 9-nm particles was proportional to the level of GAT1 expression (Fig. 8b, c). After correction for the thickness of the platinum coat, the GAT1 particle size corresponded to an integral membrane protein complex composed of 24 ± 2 transmembrane helices. Assuming 12 transmembrane helices per monomeric GAT1 (Bennett & Kanner, 1997; Clark, 1997; Yamashita et al., 2005), the GAT1 freeze-fracture particles suggested a dimeric assembly of GAT1 in the oocyte plasma membrane. Moreover, assuming that the GAT1 functional unit is the monomer (Soragna et al., 2005b; Yamashita et al., 2005), the results suggest an apparent valence ($z\delta$) of 4 ± 1 elementary charges per GAT1 monomer.

Discussion

The purpose of the present study was to obtain a reliable estimate of the physiological turnover rate of the GABA transporter GAT1. We used the *X. laevis* oocyte expression system and correlated macroscopic assays of GAT1 function and electron microscopic estimates of the total number of GAT1 copies in the plasma membrane in individual GAT1-expressing cells. In what follows, we describe how the experimental data presented in this study were used to obtain an estimate of the physiological turnover rate of GAT1.

Expression of GAT1 in the Plasma Membrane

Determination of the unitary turnover rate of GAT1 requires knowledge of the oligomeric assembly of the transporter. We used freeze-fracture and electron microscopy to examine the oligomeric assembly of GAT1 in the *X. laevis* oocyte plasma membrane. Expression of GAT1 in *X. laevis* oocytes led to the appearance of a distinct population of 9-nm particles in the plasma membrane (Fig. 8). The 9-nm particle represents functional GAT1 in the plasma membrane because (1) it is absent in control cells (Fig. 8a) (*see* Eskandari et al., 1998, 2000) and (2) its density is directly related to the macroscopic assay of GAT1 function (Figs. 7 and 8b, c). We have previously established that the cross-sectional area of the freeze-fracture particles of integral membrane proteins provides an estimate of the total number of transmembrane α-helices, which when combined with available topology information, provides an estimate of the oligomeric assembly (Eskandari et al., 1998). Assuming that GAT1 has 12 membrane-spanning domains and that these are α-helical in nature (Bennett & Kanner, 1997; Clark, 1997; Yamashita et al., 2005), the cross-sectional area of GAT1 freeze-fracture particles suggested a packing assembly of 24 α-helices. Thus, the 9-nm freeze-fracture particle induced by GAT1 expression likely represents GAT1 dimers in the plasma membrane. This finding is consistent with numerous reports suggesting an oligomeric assembly of Na^+/Cl^--coupled transporters such as the GABA, serotonin, norepinephrine and dopamine transporters (Schmid et al., 2001; Scholze, Freissmuth & Sitte, 2002; Sitte & Freissmuth, 2003; Soragna et al., 2005b; Farhan, Freissmuth & Sitte, 2006). It is also consistent with the crystallographic information obtained for a related bacterial leucine transporter ($LeuT_{Aa}$), in which the transporter was found to crystallize as a dimer (Yamashita et al., 2005). Thus, in estimating the turnover rate, we will assume that the 9-nm freeze-fracture particles induced by GAT1 expression represent GAT1 dimers.

It is also important to know the functional unit of GAT1. Recent data obtained with rGAT1 suggest that despite oligomer formation in the plasma membrane, each monomer functions independently (Soragna et al., 2005b). In addition, strong evidence was provided by the crystal structure of $LeuT_{Aa}$, which demonstrated Na^+ and substrate binding sites within the monomeric unit (Yamashita et al., 2005). Remarkably, the $LeuT_{Aa}$ structure revealed that the two Na^+ ions and the leucine substrate share the same permeation pathway. Thus, in our estimate of the turnover rate, we will assume that the functional unit of GAT1 is the GAT1 monomer.

Apparent Valence of GAT1 Moveable Charge

In individual GAT1-expresssing cells, we used the two-electrode voltage-clamp method to measure the voltage-induced transporter charge movements (Q_{NaCl}) as well as the whole-cell capacitance, as well as freeze-fracture and electron microscopy to estimate the total number of GAT1 particles in the plasma membrane. As discussed above, the GAT1 intramembrane particles most likely represent GAT1 dimers in the plasma membrane. The correlation between Q_{NaCl} and the total number of GAT1 particles in the plasma membrane yielded an apparent valence ($z\delta$) of 8 $\pm$ 1 elementary charges per GAT1 intramembrane particle and, thus, 4 $\pm$ 1 elementary charges per GAT1 monomer. This number is significantly higher than that obtained from the fit of the Q-V relationship with a single Boltzmann function (equation 3), which yields a value of unity for GAT1 $z\delta$ (*see* Fig. 1b) (Mager et al., 1993, 1996; Lu & Hilgemann, 1999b; Loo et al., 2000; Forlani et al., 2001a; Fesce et al., 2002; Whitlow et al., 2003). Additional Boltzmann states may be used to fit the data and may predict the effective valence to be slightly larger than unity (Lu & Hilgemann, 1999b; Krofchick, Huntley & Silverman, 2004), but these values still underestimate the value obtained using our direct method. A similar discrepancy between the electrophysiological and freeze-fracture estimates of the effective valence was reported for the Na^+/glucose and Na^+/iodide cotransporters and the *Shaker* K^+ channel (Zampighi et al., 1995; Eskandari et al., 1997). For the Na^+/glucose and Na^+/iodide cotransporters, the apparent valence values obtained from freeze-fracture experiments were 3.5 and 3, respectively, whereas the electrophysiological values were unity for both transporters (obtained from a single Boltzmann fit of the charge-voltage relationship) (Zampighi et al., 1995; Eskandari et al., 1997). In the case of the *Shaker* K^+ channel, the apparent valence determined by the freeze-fracture method was 9 (Zampighi et al., 1995), while the electrophysiological measurement of the macroscopic gating currents required fitting the charge-voltage relationship with a sum of two Boltzmann functions, yielding z values of 1.6 and 4.6 (using the cut-open oocyte voltage-clamp technique; Bezanilla & Stefani, 1998). It is now accepted that the voltage sensor of the *Shaker* K^+ channel moves about 12–13 elementary charges across the entire membrane electric field (Bezanilla, 2000, 2002). Thus, it is plausible to suggest that electrophysiological measurements of macroscopic charge movements may underestimate the true charge moved across the membrane electric field per functional transporter.

Based on the available data, it is difficult to reconcile the apparent valence of four elementary charges with the known stoichiometry of GAT1 (2 Na^+:1 Cl^-:1 GABA). We speculate that our measured apparent valence represents charge movements contributed by Na^+ and Cl^- ions that enter the membrane electric field, as well as charge movements that arise from dipole movements linked to conformational changes of the transporter. We predict that these charge movements are complex events, and a combination of biophysical and structural data is required to fully understand them.

Turnover Rate of GAT1

To understand the role played by GAT1 at fast GABAergic synapses, it is imperative that we know the rate at which this transporter removes GABA from the synapse. A transport cycle of GAT is defined as the conformational changes required for the movement of one GABA molecule across the plasma membrane (Hilgemann & Lu, 1999), and the unitary turnover rate (R) is defined as the number of GABA molecules translocated across the plasma membrane per unit time, generally expressed in cycles per second. A common approach used to estimate the unitary turnover rate of electrogenic Na^+-coupled transporters is to plot the maximum steady-state macroscopic substrate-evoked current ($I_{max} = N_T meR_T$, *see* "Introduction") as a function of transporter-mediated charge movements in response to a series of voltage pulses ($Q_{max} = N_T z\delta e$) (*see* Fig. 1d) (e.g., *see* Loo et al., 1993; Mager et al., 1993; Forlani et al., 2001a; Sacher et al., 2002; Karakossian et al., 2005). The slope of the I_{max}-Q_{max} plot ($Slope_{I-Q}$) is then taken as the turnover rate of the transport cycle (Fig. 1d) (Loo et al., 1993; Mager et al., 1993).

As shown in "Results" and discussed below, it is not always feasible to measure I_{max} under experimental conditions suitable for *X. laevis* oocytes, and, in fact for GAT1, the measured I_{NaCl}^{GABA} is a fraction of I_{max} under most conditions (Fig. 4). To account for subsaturating concentrations of cosubstrates, the Na^+- and Cl^--coupled GABA-evoked current (I_{NaCl}^{GABA}in amperes) mediated by GAT1 may be redefined as follows:

$$I_{NaCl}^{GABA} = f_I N_T meR_T \quad (4)$$

where f_I is the fraction of the maximum evoked current (I_{max}) and is a function of the cosubstrate concentrations (*see* equation 5), N_T is the total number of functional transporters in the plasma membrane, m is the number of charges translocated across the plasma membrane per transport cycle, e is the elementary charge ($e = 1.602 \times 10^{-19}$ C) and R_T is the unitary transporter turnover rate (cycles per second). f_I is a function of the concentrations of the cosubstrates Na^+, Cl^- and GABA and can be empirically approximated by a combined Michaelis-Menten and Hill relationship:

$$f_I = \left(\frac{[Na]^n}{(K_{0.5}^{Na})^n + [Na]^n}\right) \times \left[I_{Cl} \times \left(\frac{[Cl]}{K_{0.5}^{Cl} + [Cl]}\right) + I_{Cl=0}\right] \times \left(\frac{[GABA]}{K_{0.5}^{GABA} + [GABA]}\right) \quad (5)$$

where $K_{0.5}^{Na}$ is the half-maximal concentration for Na^+ (65 mM at −50 m*V*), *n* is the Na^+ Hill coefficient ($n = 2$), $K_{0.5}^{Cl}$ is the half-maximal concentration for Cl^- (47 mM at −50 m*V*), $I_{Cl=0}$ is the fraction of the GABA-evoked current present in the absence of external Cl^- ($I_{Cl=0} = 0.3$, *see* Fig. 3e), I_{Cl} is the fraction of the current enhanced by saturating external Cl^- concentration ($I_{Cl} = 0.7$) and $K_{0.5}^{GABA}$ is the half-maximal concentration for GABA (26 μM at −50 m*V*). The Na^+, Cl^- and GABA concentrations are expressed in the same unit as the corresponding $K_{0.5}$ values. This equation adequately describes the dependence of GAT1-mediated macroscopic current (I_{NaCl}^{GABA}) on the external concentrations of the cosubstrates (Na^+, Cl^- and GABA) (*see* Fig. 4). It is readily seen that no current is evoked in the absence of either Na^+ or GABA (Fig. 3a, b), consistent with the strict dependence of GAT1 on external Na^+ and a lack of leak current in the absence of GABA (Lu & Hilgemann, 1999a; Loo et al., 2000; Karakossian et al., 2005). Increasing the concentration of Na^+ and GABA increases the evoked GAT1-mediated current according to the corresponding Hill or Michaelis-Menten relationship. It is also readily seen that in the absence of external Cl^-, the evoked current is 30% of I_{max} and is consistent with a lack of absolute dependence of GAT1 on external chloride (*see* Fig. 3e; Kavanaugh et al., 1992; Keynan et al., 1992; Loo et al., 2000). At saturating concentrations of Na^+, Cl^- and GABA, $f_I = 1$ and, thus, $I_{NaCl}^{GABA} = I_{max}$. At –50 m*V* and under our experimental conditions in *X. laevis* oocytes (100 mM $[Na^+]_o$, 106 mM $[Cl^-]_o$ and 5 mM [GABA]), $f_I = 0.55$. As the half-maximal concentration values for Na^+, Cl^- and GABA are voltage-dependent, f_I is also voltage-dependent (*see* Table 1) (Mager et al., 1993; Forlani et al., 2001a; Soragna et al., 2005a).

Compared to GAT1, the closely related mouse GAT3 isoform (mGAT3) exhibits a higher apparent affinity for Na^+ (14 mM), Cl^- (1 mM) and GABA (3 μM) (Sacher et al., 2002; Whitlow et al., 2003). At 100 mM Na^+, 106 mM Cl^- and 1 mM GABA, equation 5 predicts that I_{NaCl}^{GABA} mediated by mGAT3 is 97% of I_{max}. Consistent with this prediction, no significant increase was observed in mGAT3 I_{NaCl}^{GABA} when the Na^+ and Cl^- concentrations were increased from 100 to 150 mM (*not shown*).

The transporter-mediated charge movements (Q_{max}) are recorded in the absence of the organic substrate but in the presence of saturating concentrations of the required driving ion (Na^+ for Na^+-driven cotransporters, H^+ for H^+-driven cotransporters). It is also important that charge movement measurements are recorded over a wide enough voltage range to ensure adequate measurement of the total charge. For GAT1, the charge movements strongly depend on the external Na^+ concentration (*not shown* for hGAT1, but see Mager et al., 1996, for rGAT1). The total charge moved is independent of the external Cl^- concentration (Mager et al., 1993, 1996; Loo et al., 2000). Under our standard concentrations of 100 mM Na^+, 106 mM Cl^- and absence of GABA and a voltage range of –150 to +60 m*V*, the measured charge (Q_{NaCl}) adequately represents the total charge; $Q_{NaCl} \approx Q_{max}$ (Mager et al., 1993, 1996).

We can now reexamine the relationship between the GAT1 substrate-evoked current (I_{NaCl}^{GABA}) and transporter-mediated charge movements (Q_{NaCl}), henceforth referred to as the *I-Q* relationship (Fig. 1d):

$$Slope_{I-Q} = \frac{I_{NaCl}^{GABA}}{Q_{NaCl}} = \frac{f_I N_T m e R_T}{N_T z\delta e} \quad (6)$$

After simplifying and rearranging to solve for R_T, we obtain the following:

$$R_T = \frac{Slope_{I-Q} z\delta}{f_I m} \quad (7)$$

We have experimentally determined the values of $Slope_{I\text{-}Q}$ (4.2 s^{-1} at –50 m*V* and 21°C, *see* Fig. 1d and Table 1), *m* (*m* = 2, Fig. 2d–f) and $z\delta$ ($z\delta = 4$), and under our experimental conditions, $f_I = 0.55$ (at –50 m*V*). Substituting these values in equation 7 yields a GAT1 unitary turnover rate of 15 ± 2 s^{-1} at 21°C and –50 m*V*. This estimate of the GAT1 turnover rate is higher than that reported in most previous investigations (Radian et al., 1986; Mager et al., 1993; Forlani et al., 2001b; Fesce et al., 2002) but closer to that reported in a recent study utilizing rapid concentration jumps for rat GAT1 (13 s^{-1} at –40 m*V* and room temperature; Bicho & Grewer, 2005).

In order to estimate the physiological turnover rate of GAT1, it is also necessary to define the voltage and temperature dependence of R_T. $z\delta$ and *m* are voltage-independent (Fig. 2d–f) (Binda et al., 2002). I_{NaCl}^{GABA} and the half-maximal concentration values for cosubstrates ($K_{0.5}^{Na}$, $K_{0.5}^{Cl}$ and $K_{0.5}^{GABA}$) are voltage-dependent (Fig. 2c and Table 1), leading to voltage dependence of $Slope_{I\text{-}Q}$ and f_I, respectively (Table 1). The voltage dependence of $Slope_{I\text{-}Q}$ and f_I can, therefore, be used to estimate the turnover rate over a limited voltage range of –90 to –10 m*V* (Table 1). For example, at 21°C, the GAT1 unitary turnover rate was estimated to be 6 ± 1 s^{-1} at –10 m*V* and 18 ± 3 s^{-1} at –90 m*V* (Fig. 9 and Table 1).

While the macroscopic current of GAT1 (I_{NaCl}^{GABA}) is temperature-dependent, the charge movements (Q_{NaCl} and thus $z\delta$), the number of charges translocated per transport

cycle (m) and the half-maximal concentration values ($K_{0.5}^{Na}$, $K_{0.5}^{Cl}$ and $K_{0.5}^{GABA}$) exhibit no apparent temperature dependence (Figs. 2d–f, 3) (Binda et al., 2002). Thus, of the parameters of equation 7, only $Slope_{I\text{-}Q}$ appears to be temperature-dependent. At 21°C, the experimentally determined values of $Slope_{I\text{-}Q}$ are shown in Table 1. At other temperatures, $Slope_{I\text{-}Q}$ may be calculated according to the following:

$$Slope_{I-Q}(T) = (Slope_{I-Q})_{21^\circ C} \times Q_{10}^{\frac{T-21}{10}} \quad (8)$$

where $Slope_{I\text{-}Q}$ values at 21°C are shown in Table 1, T is temperature (range 19–37°C) and Q_{10} is 2.8 ± 0.1 for hGAT1 (Fig. 2a). Using this equation and the information provided in Table 1, we can estimate the turnover rate of GAT1 at 37°C and voltages ranging from –90 to –10 mV. For example, at 37°C, the GAT1 turnover rate is estimated to be 79 ± 11 s^{-1} at –50 mV and 93 ± 13 s^{-1} at –90 mV (Fig. 9 and Table 1). Thus, on average, a complete transport cycle lasts ~11 ms (–90 mV) to ~13 ms (–50 mV).

Although the experimental temperature range for equation 8 is 19–32°C, the linearity of the Arrhenius plot (Fig. 2b) suggests that the temperature range may be extrapolated to 37°C. At temperatures below 17°C, the Arrhenius plot deviated from linearity (*not shown*). It is also important to note that the conditions in the above analysis refer to zero-*trans* GABA (extracellular GABA at the indicated concentration and negligible cytoplasmic GABA), and future experiments are needed to quantify R_T when the zero-*trans* condition is not met. Finally, as the cytoplasmic concentrations of Na^+ and Cl^- may vary in different cells, future experiments should address the role played by cytoplasmic Na^+ and Cl^- in modulating the turnover rate of GAT1 (Lu et al., 1995; Lu & Hilgemann, 1999a).

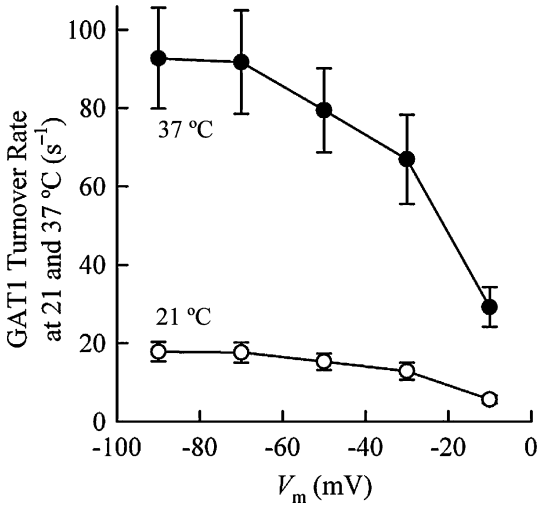

Fig. 9 Predicted physiological turnover rate of GAT1. Equations 5, 7 and 8 and the information provided in Table 1 were used to estimate the physiological turnover rate of GAT1 at 21°C (*open circles*) and 37°C (*filled circles*) and membrane potentials ranging from –90 to –10 mV

Analysis of Intrinsic Assumptions and Potential Sources of Error

It is important that we evaluate the intrinsic assumptions as well as the potential sources of error in our study. Examination of equations 4–8 allows us to determine how an error or a deviation from a given assumption would alter the estimated turnover rate.

The $z\delta$ obtained per GAT1 freeze-fracture particle was 8 ± 1 (i.e., 8 unitary charges per GAT1 intramembrane particle). As we have assumed the functional transporter unit to be the GAT1 monomer, we used a value of 4 for $z\delta$ in equation 7. If it turns out that the dimer is the functional unit, then our estimates of the turnover rate at 21°C need to be multiplied by a factor of 2.

It is important to establish that our method can account for all of the GAT1 copies in the plasma membrane. To this end, we determined that the density of the newly inserted particles in the plasma membrane is uniform regardless of the region sampled on the cell surface. Moreover, that there is a strong correlation between Q_{NaCl} and the number of transporters in the plasma membrane also suggests that the density is uniform and may be sampled from any region of the plasma membrane (Fig. 7). Approximately 80–90% of the oocyte plasma membrane is in the microvilli (Zampighi et al., 1995; Zhang & Hamill, 2000). Because the plane of the plasma membrane in microvilli is highly curved, in most freeze-fracture replicas, we were unable to accurately quantify the density in microvilli. In these regions, the number of particles could be quantified but the membrane curvature caused an error in the measured area, leading to higher density estimates than those found in flat regions of the plasma membrane. However, when relatively flat regions of initial regions of microvilli were examined, the density was not different from that in other flat regions of the plasma membrane (*not shown*). It is important to note that the density measurements in the microvilli were always significantly higher than those found in flat regions of the plasma membrane and that we never observed microvilli regions in which the particle density was at or below that in other flat regions of the plasma membrane. We attribute these artificially high density measurements to the curvature of the microvilli plasma membrane, and we have no reason to believe that GAT1 expression in the microvilli is different from that in other regions of the plasma membrane. Finally, consistent with previous reports (Zampighi et al., 1995; Eskandari et al., 1997, 1998, 1999, 2000), we did not see any evidence of GAT1 particles in

the E face of the plasma membrane. Thus, all in all, we believe that our combined electrophysiology (using whole-cell capacitance to yield the total surface area of the plasma membrane) and freeze-fracture (yielding the average GAT1 density) methods provide a good estimate of the total number of plasma membrane transporters per *X. laevis* oocyte.

Do all newly inserted freeze-fracture particles represent functional GAT1 copies in the plasma membrane? Expression of GAT1 induced the appearance of a 9-nm freeze-fracture particle (Fig. 8), however, it is not possible to ascertain that all of the newly inserted particles are GAT1 or that they are all functional GAT1. If functional GABA transporters in the oocyte plasma membrane represent a fraction of the total number of newly inserted particles, then a smaller than measured population of GABA transporters is responsible for the recorded macroscopic signal, and our reported turnover rate would represent an underestimate of the true turnover rate.

Although we have attempted to sample our density measurements from flat regions of the membrane (as judged by short shadows of the intramembrane particles), it is virtually impossible to find perfectly flat regions of the plasma membrane, and some local curvature in the plasma membrane is usually present. This becomes particularly apparent when stereoscopic images are obtained (*not shown*). Although it is difficult to estimate the extent to which this factor would contribute to an error, the local curvature invariably leads to an underestimation of the area, which causes an overestimation of the density and, hence, the total number of transporters. Overestimation of the total number of transporters leads to underestimation of $z\delta$, which ultimately leads to underestimation of the unitary turnover rate.

Does the two-electrode voltage-clamp method have sufficient time resolution to measure all of the voltage-induced transporter charge movement (Q_{NaCl})? Using giant membrane patches, a fast charge moving reaction (Q_{fast}) was shown to be responsible for as much as 10% of the total charge moved by GAT1 (Lu et al., 1995; Lu & Hilgemann, 1999b). This component is too fast to be resolved by the two-electrode voltage-clamp method. Thus, our measured Q_{NaCl} may underestimate the total charge by $\sim$10%. If this is taken into account, it leads to an increase in the value of $z\delta$ per functional GAT1 by 10%, which will require us to increase our estimated turnover rate by $\sim$10%. We have not corrected our turnover rate estimates to take this factor into account.

Does the density of endogenous intramembrane particles remain constant when the total surface area increases upon expression of GAT1 in the plasma membrane? In determining the number of GAT1 in the plasma membrane, we subtracted the density of endogenous particles from the density in GAT-expressing cells. We did this with the assumption that the density of endogenous particles remains the same as additional membrane is added to the plasma membrane in GAT1-expressing cells. This may be a reasonable assumption as the endogenous density remained the same over a wide range of capacitance measurements in control cells (170–340 nF).

In estimating the total surface area of the plasma membrane, we used a specific membrane capacitance of 1 $\mu F/cm^2$ (Zampighi et al., 1995; Hirsch et al., 1996; Forster et al., 1999; Zhang & Hamill, 2000). However, some investigators have used values as low as 0.7 $\mu F/cm^2$ (e.g., Baumgartner, Islas & Sigworth, 1999). Thus, it is possible that we underestimated the total number of transporters, which in turn overestimates the value of $z\delta$ and ultimately leads to overestimation of the unitary turnover rate by as much as 30%. If 0.7 $\mu F/cm^2$ is used, the predicted turnover rate will be 11 s^{-1} (at 21°C and –50 m*V*), and when extrapolated to the physiological range, the turnover rate ranges from 56 to 65 s^{-1} at 37°C and membrane potentials ranging from –50 to –90 m*V*.

Physiological Significance

It has been known for two decades that specific inhibition of GAT1 by compounds such as NO-711, SKF 89976-A and tiagabine in native preparations leads to significant prolongation of the postsynaptic response at GABAergic synapses (Dingledine & Korn, 1985; Roepstorff & Lambert, 1992, 1994; Thompson & Gähwiler, 1992; Isaacson, Solis & Nicoll, 1993; Draguhn & Heinemann, 1996; Engel et al., 1998; Rossi & Hamann, 1998; Overstreet, Jones & Westbrook, 2000; Overstreet & Westbrook, 2003; Keros & Hablitz, 2005). These observations suggested either that GAT1 is found at very high densities in synaptic regions or that it has a high turnover rate, or both. After cloning of GAT1 in 1990 (Guastella et al., 1990; Nelson et al., 1990), application of electrophysiological methods estimated the turnover rate to be 1.2–10.4 s^{-1} (at 22°C and voltages ranging from –20 to –140 m*V*) (Mager et al., 1993). This result raised an important question as to how, despite the low turnover rate, this transporter is effective at clearing GABA at fast GABAergic synapses, where inhibitory postsynaptic currents decay with time constants of $\leq$10 ms. Additional data were presented when the density of GAT1 was estimated to be high ($\sim$800/μm^2) in synaptic regions (Chiu et al., 2002); however, recent estimates suggest lower densities of 300–400 transporters/μm^2 in the plasma membrane (Wang & Quick, 2005). However, acute trafficking events may lead to the delivery or retrieval of large numbers of transporters within tens of seconds to the cell surface (Wang & Quick, 2005). Here, our data suggest that

the turnover rate of GAT1 is 79–93 s^{-1} (at 37°C and –50 to –90 m*V*), suggesting that, on average, a complete transport cycle lasts 11–13 ms. Thus, the clearance rate predicted by our estimate of the turnover rate is in agreement with the experimentally observed role of GAT1 in shaping postsynaptic responses in native preparations. We propose that both the rapid turnover rate of GAT1 and dynamic regulation of transporter surface density at fast GABAergic synapses lead to the effectiveness of this transporter in shaping the postsynaptic responses mediated by $GABA_A$ receptors.

For the glutamate transporters, it has been predicted that rapid substrate binding followed by rapid translocation across the plasma membrane may be responsible for the initial "buffering" of synaptically released glutamate, although the return of the empty binding sites to the extracellular surface may be the rate-limiting step in the transport cycle (Grewer et al., 2000; Otis & Kavanaugh, 2000; Watzke, Bamberg & Grewer, 2001). There is some evidence that this may also be the case with the GABA transporters as rapid application of GABA leads to fast electrogenic events that may represent rapid binding and translocation of the substrate (Cammack et al., 1994; Bicho & Grewer, 2005; Karakossian et al., 2005).

When GAT1-specific currents are recorded in native preparations, equations 4 and 5 and the information presented in Table 1 may be used to estimate the number of transporters that give rise to the recorded signal. Thus, our data may pave the way for a better characterization of GAT1 densities in the plasma membrane of native cells. In addition, in heterologous expression systems, either the measured GABA-evoked current ($I_{NaCl}^{GABA} = f_I N_T m e R_T$) or the voltage-induced charge movements ($Q_{NaCl} = N_T z \delta e$) can be used to provide a reasonable estimate of the total number of functional transporters at the cell surface.

Conclusions

In summary, we have shown that in the absence of experimental determination of the values of m and $z\delta$ in electrogenic Na^+-coupled cotransporters, the slope of the plot I_{max}/Q_{max} is not a reliable predictor of the transporter turnover rate. Moreover, it must be experimentally established that the measured I_{max} and Q_{max}, in fact, represent the maximum transport rate and charge movements, respectively. When all of these factors were taken into account, our data suggest that GAT1 has a higher turnover rate than previously estimated based solely on electrophysiological methods. We estimate a GAT1 unitary turnover rate that ranges 79–93 s^{-1} at 37°C and membrane potentials from –50 to –90 m*V*. These results provide molecular justification for the well-documented role of GAT1 as an effective regulator of the concentration and lifetime of GABA at fast GABAergic synapses.

Acknowledgement We thank Dr. Donald D. F. Loo (Department of Physiology, David Geffen School of Medicine at UCLA, Los Angeles, CA) for his insightful comments on this manuscript and Gail M. Drus and Michael J. Errico for technical assistance. This work was supported by a U.S. National Institutes of Health grant awarded to S. E. (S06 GM53933). J. Y. K. was supported by the Howard Hughes Medical Institute–Cal Poly Pomona Undergraduate Research Apprentice Program, 2004–2008.

References

Bacconi A, Ravera S, Virkki LV, Murer H, Forster IC (2007) Temperature dependence of steady-state and presteady-state kinetics of a type IIb Na^+/P_i cotransporter. J Membr Biol 215:81–92

Baumgartner W, Islas L, Sigworth FJ (1999) Two-microelectrode voltage clamp of *Xenopus* oocytes: voltage errors and compensation for local current flow. Biophys J 77:1980–1991

Bennett ER, Kanner BI (1997) The membrane topology of GAT-1, a (Na^+ + Cl^-)-coupled γ-aminobutyric acid transporter from rat brain. J Biol Chem 272:1203–1210

Bezanilla F (2000) The voltage sensor in voltage-dependent ion channels. Physiol Rev 80:555–592

Bezanilla F (2002) Voltage sensor movements. J Gen Physiol 120:465–473

Bezanilla F, Stefani E (1998) Gating currents. Methods Enzymol 293:331–352

Bicho A, Grewer C (2005) Rapid substrate-induced charge movements of the GABA transporter GAT1. Biophys J 89:211–231

Binda F, Bossi E, Giovannardi S, Forlani G, Peres A (2002) Temperature effects on the presteady-state and transport-associated currents of GABA cotransporter rGAT1. FEBS Lett 512:303–307

Borden LA (1996) GABA transporter heterogeneity: pharmacology and cellular localization. Neurochem Int 29:335–356

Bron P, Lagrée V, Froger A, Rolland JP, Hubert JF, Delamarche C, Deschamps S, Pellerin I, Thomas D, Haase W (1999) Oligomerization state of MIP proteins expressed in *Xenopus* oocytes as revealed by freeze-fracture electron-microscopy analysis. J Struct Biol 128:287–296

Cammack JN, Rakhilin SV, Schwartz EA (1994) A GABA transporter operates asymmetrically and with variable stoichiometry. Neuron 13:949–960

Chandy G, Zampighi GA, Kreman M, Hall JE (1997) Comparison of the water transporting properties of MIP and AQP1. J Membr Biol 159:29–39

Chen NH, Reith ME, Quick MW (2004) Synaptic uptake and beyond: the sodium- and chloride-dependent neurotransmitter transporter family SLC6. Pfluegers Arch 447:519–531

Chiu CS, Jensen K, Sokolova I, Wang D, Li M, Deshpande P, Davidson N, Mody I, Quick MW, Quake SR, Lester HA (2002) Number, density, and surface/cytoplasmic distribution of GABA transporters at presynaptic structures of knock-in mice carrying GABA transporter subtype 1-green fluorescent protein fusions. J Neurosci 22:10251–10266

Clark JA (1997) Analysis of the transmembrane topology and membrane assembly of the GAT-1 γ-aminobutyric acid transporter. J Biol Chem 272:14695–14704

Conti F, Minelli A, Melone M (2004) GABA transporters in the mammalian cerebral cortex: localization, development and pathological implications. Brain Res Brain Res Rev 45:196–212

Dalby NO (2003) Inhibition of γ-aminobutyric acid uptake: anatomy, physiology and effects against epileptic seizures. Eur J Pharmacol 479:127–137

Deken SL, Beckman ML, Boos L, Quick MW (2000) Transport rates of GABA transporters: regulation by the N-terminal domain and syntaxin 1A. Nat Neurosci 3:998–1003

Dingledine R, Korn SJ (1985) γ-Aminobutyric acid uptake and the termination of inhibitory synaptic potentials in the rat hippocampal slice. J Physiol 366:387–409

Draguhn A, Heinemann U (1996) Different mechanisms regulate IPSC kinetics in early postnatal and juvenile hippocampal granule cells. J Neurophysiol 76:3983–3993

Engel D, Schmitz D, Gloveli T, Frahm C, Heinemann U, Draguhn A (1998) Laminar difference in GABA uptake and GAT-1 expression in rat CA1. J Physiol 512:643–649

Eskandari S, Loo DDF, Dai G, Levy O, Wright EM, Carrasco N (1997) Thyroid Na^+/I^- symporter. Mechanism, stoichiometry, and specificity. J Biol Chem 272:27230–27238

Eskandari S, Wright EM, Kreman M, Starace DM, Zampighi GA (1998) Structural analysis of cloned plasma membrane proteins by freeze-fracture electron microscopy. Proc Natl Acad Sci USA 95:11235–11240

Eskandari S, Snyder PM, Kreman M, Zampighi GA, Welsh MJ, Wright EM (1999) Number of subunits comprising the epithelial sodium channel. J Biol Chem 274:27281–27286

Eskandari S, Kreman M, Kavanaugh MP, Wright EM, Zampighi GA (2000) Pentameric assembly of a neuronal glutamate transporter. Proc Natl Acad Sci USA 97:8641–8646

Farhan H, Freissmuth M, Sitte HH (2006) Oligomerization of neurotransmitter transporters: a ticket from the endoplasmic reticulum to the plasma membrane. Handb Exp Pharmacol 175:233–249

Fesce R, Giovannardi S, Binda F, Bossi E, Peres A (2002) The relation between charge movement and transport-associated currents in the rat GABA cotransporter rGAT1. J Physiol 545:739–750

Forlani G, Bossi E, Ghirardelli R, Giovannardi S, Binda F, Bonadiman L, Ielmini L, Peres A (2001a) Mutation K448E in the external loop 5 of rat GABA transporter rGAT1 induces pH sensitivity and alters substrate interactions. J Physiol 536:479–494

Forlani G, Bossi E, Perego C, Giovannardi S, Peres A (2001b) Three kinds of currents in the canine betaine-GABA transporter BGT-1 expressed in *Xenopus laevis* oocytes. Biochim Biophys Acta 1538:172–180

Forster IC, Kohler K, Biber J, Murer H (2002) Forging the link between structure and function of electrogenic cotransporters: the renal type IIa Na^+/P_i cotransporter as a case study. Prog Biophys Mol Biol 80:69–108

Forster IC, Traebert M, Jankowski M, Stange G, Biber J, Murer H (1999) Protein kinase C activators induce membrane retrieval of type II Na^+-phosphate cotransporters expressed in *Xenopus* oocytes. J Physiol 517:327–340

Grewer C, Watzke N, Wiessner M, Rauen T (2000) Glutamate translocation of the neuronal glutamate transporter EAAC1 occurs within milliseconds. Proc Natl Acad Sci USA 97:9706–9711

Guastella J, Nelson N, Nelson H, Czyzyk L, Keynan S, Miedel MC, Davidson N, Lester HA, Kanner BI (1990) Cloning and expression of a rat brain GABA transporter. Science 249:1303–1306

Gutfreund H (1995) Kinetics for the life sciences. Receptors, transmitters and catalysts. Cambridge University Press, New York

Hansra N, Arya S, Quick MW (2004) Intracellular domains of a rat brain GABA transporter that govern transport. J Neurosci 24:4082–4087

Hazama A, Loo DDF, Wright EM (1997) Presteady-state currents of the rabbit Na^+/glucose cotransporter (SGLT1). J Membr Biol 155:175–186

Hilgemann DW, Lu CC (1999) GAT1 (GABA:Na^+:Cl^-) cotransport function. Database reconstruction with an alternating access model. J Gen Physiol 114:459–475

Hirsch JR, Loo DDF, Wright EM (1996) Regulation of Na^+/glucose cotransporter expression by protein kinases in *Xenopus laevis* oocytes. J Biol Chem 271:14740–14746

Isaacson JS, Solis JM, Nicoll RA (1993) Local and diffuse synaptic actions of GABA in the hippocampus. Neuron 10:165–175

Isom LL, Ragsdale DS, De Jongh KS, Westenbroek RE, Reber BF, Scheuer T, Catterall WA (1995) Structure and function of the β2 subunit of brain sodium channels, a transmembrane glycoprotein with a CAM motif. Cell 83:433–442

Karakossian MH, Spencer SR, Gomez AQ, Padilla OR, Sacher A, Loo DDF, Nelson N, Eskandari S (2005) Novel properties of a mouse γ-aminobutyric acid transporter (GAT4). J Membr Biol 203:65–82

Kavanaugh MP, Arriza JL, North RA, Amara SG (1992) Electrogenic uptake of γ-aminobutyric acid by a cloned transporter expressed in *Xenopus* oocytes. J Biol Chem 267:22007–22009

Keros S, Hablitz JJ (2005) Subtype-specific GABA transporter antagonists synergistically modulate phasic and tonic $GABA_A$ conductances in rat neocortex. J Neurophysiol 94:2073–2085

Keynan S, Suh YJ, Kanner BI, Rudnick G (1992) Expression of a cloned γ-aminobutyric acid transporter in mammalian cells. Biochemistry 31:1974–1979

Krause S, Schwarz W (2005) Identification and selective inhibition of the channel mode of the neuronal GABA transporter 1. Mol Pharmacol 68:1728–1735

Krofchick D, Huntley SA, Silverman M (2004) Transition states of the high-affinity rabbit Na^+/glucose cotransporter SGLT1 as determined from measurement and analysis of voltage-dependent charge movements. Am J Physiol 287:C46–C54

Loo DDF, Hazama A, Supplisson S, Turk E, Wright EM (1993) Relaxation kinetics of the Na^+/glucose cotransporter. Proc Natl Acad Sci USA 90:5767–5771

Loo DDF, Eskandari S, Boorer KJ, Sarkar HK, Wright EM (2000) Role of Cl^- in electrogenic Na^+-coupled cotransporters GAT1 and SGLT1. J Biol Chem 275:37414–37422

Lu CC, Hilgemann DW (1999a) GAT1 (GABA:Na^+:Cl^-) cotransport function. Steady state studies in giant *Xenopus* oocyte membrane patches. J Gen Physiol 114:429–444

Lu CC, Hilgemann DW (1999b) GAT1 (GABA:Na^+:Cl^-) cotransport function. Kinetic studies in giant *Xenopus* oocyte membrane patches. J Gen Physiol 114:445–457

Lu CC, Kabakov A, Markin VS, Mager S, Frazier GA, Hilgemann DW (1995) Membrane transport mechanisms probed by capacitance measurements with megahertz voltage clamp. Proc Natl Acad Sci USA 92:11220–11224

Mackenzie B, Loo DDF, Fei YJ, Liu W, Ganapathy V, Leibach FH, Wright EM (1996) Mechanisms of the human intestinal H^+-coupled oligopeptide transporter hPEPT1. J Biol Chem 271:5430–5437

Mager S, Naeve J, Quick M, Labarca C, Davidson N, Lester HA (1993) Steady states, charge movements, and rates for a cloned GABA transporter expressed in *Xenopus* oocytes. Neuron 10:177–188

Mager S, Kleinberger-Doron N, Keshet GI, Davidson N, Kanner BI, Lester HA (1996) Ion binding and permeation at the GABA transporter GAT1. J Neurosci 16:5405–5414

Mim C, Balani P, Rauen T, Grewer C (2005) The glutamate transporter subtypes EAAT4 and EAATs 1–3 transport glutamate with dramatically different kinetics and voltage dependence but share a common uptake mechanism. J Gen Physiol 126:571–589

Nelson N (1998) The family of Na^+/Cl^- neurotransmitter transporters. J Neurochem 71:1785–1803

Nelson H, Mandiyan S, Nelson N (1990) Cloning of the human brain GABA transporter. FEBS Lett 269:181–184

Otis TS, Kavanaugh MP (2000) Isolation of current components and partial reaction cycles in the glial glutamate transporter EAAT2. J Neurosci 20:2749–2757

Overstreet LS, Jones MV, Westbrook GL (2000) Slow desensitization regulates the availability of synaptic $GABA_A$ receptors. J Neurosci 20:7914–7921

Overstreet LS, Westbrook GL (2003) Synapse density regulates independence at unitary inhibitory synapses. J Neurosci 23:2618–2626

Parent L, Supplisson S, Loo DD, Wright EM (1992) Electrogenic properties of the cloned Na^+/glucose cotransporter: II. A transport model under nonrapid equilibrium conditions. J Membr Biol 125:63–79

Parent L, Wright EM (1993) Electrophysiology of the Na+/glucose cotransporter. In: Reuss L, Russell JM Jr, Jennings ML (eds) Molecular biology and function of carrier proteins. Rockefeller University Press, New York, pp 263–281

Quick MW (2002) Substrates regulate γ-aminobutyric acid transporters in a syntaxin 1A-dependent manner. Proc Natl Acad Sci USA 99:5686–5691

Radian R, Bendahan A, Kanner BI (1986) Purification and identification of the functional sodium- and chloride-coupled γ-aminobutyric acid transport glycoprotein from rat brain. J Biol Chem 261:15437–15441

Richerson GB, Wu Y (2003) Dynamic equilibrium of neurotransmitter transporters: not just for reuptake anymore. J Neurophysiol 90:1363–1374

Roepstorff A, Lambert JD (1992) Comparison of the effect of the GABA uptake blockers, tiagabine and nipecotic acid, on inhibitory synaptic efficacy in hippocampal CA1 neurones. Neurosci Lett 146:131–134

Roepstorff A, Lambert JD (1994) Factors contributing to the decay of the stimulus-evoked IPSC in rat hippocampal CA1 neurons. J Neurophysiol 72:2911–2926

Rossi DJ, Hamann M (1998) Spillover-mediated transmission at inhibitory synapses promoted by high affinity alpha6 subunit $GABA_A$ receptors and glomerular geometry. Neuron 20:783–795

Sacher A, Nelson N, Ogi JT, Wright EM, Loo DDF, Eskandari S (2002) Presteady-state and steady-state kinetics, and turnover rate of the mouse γ-aminobutyric acid transporter (mGAT3). J Membr Biol 190:57–73

Schmid JA, Scholze P, Kudlacek O, Freissmuth M, Singer EA, Sitte HH (2001) Oligomerization of the human serotonin transporter and of the rat GABA transporter 1 visualized by fluorescence resonance energy transfer microscopy in living cells. J Biol Chem 276:3805–3810

Scholze P, Freissmuth M, Sitte HH (2002) Mutations within an intramembrane leucine heptad repeat disrupt oligomer formation of the rat GABA transporter 1. J Biol Chem 277:43682–43690

Segel IH (1975) Enzyme kinetics: behavior and analysis of rapid equilibrium and steady-state enzyme systems. Wiley, New York

Sitte HH, Freissmuth M (2003) Oligomer formation by Na^+-Cl^--coupled neurotransmitter transporters. Eur J Pharmacol 479:229–236

Soragna A, Bossi E, Giovannardi S, Pisani R, Peres A (2005a) Relations between substrate affinities and charge equilibration rates in the rat GABA cotransporter GAT1. J Physiol 562:333–345

Soragna A, Bossi E, Giovannardi S, Pisani R, Peres A (2005b) Functionally independent subunits in the oligomeric structure of the GABA cotransporter rGAT1. Cell Mol Life Sci 62:2877–2885

Thompson SM, Gähwiler BH (1992) Effects of the GABA uptake inhibitor tiagabine on inhibitory synaptic potentials in rat hippocampal slice cultures. J Neurophysiol 67:1698–1701

Trotti D, Peng JB, Dunlop J, Hediger MA (2001) Inhibition of the glutamate transporter EAAC1 expressed in *Xenopus* oocytes by phorbol esters. Brain Res 914:196–203

Wadiche JI, Arriza JL, Amara SG, Kavanaugh MP (1995) Kinetics of a human glutamate transporter. Neuron 14:1019–1027

Wang D, Deken SL, Whitworth TL, Quick MW (2003) Syntaxin 1A inhibits GABA flux, efflux, and exchange mediated by the rat brain GABA transporter GAT1. Mol Pharmacol 64:905–913

Wang D, Quick MW (2005) Trafficking of the plasma membrane γ-aminobutyric acid transporter GAT1: size and rates of an acutely recycling pool. J Biol Chem 280:18703–18709

Watzke N, Bamberg E, Grewer C (2001) Early intermediates in the transport cycle of the neuronal excitatory amino acid carrier EAAC1. J Gen Physiol 117:547–562

Whitlow RD, Sacher A, Loo DDF, Nelson N, Eskandari S (2003) The anticonvulsant valproate increases the turnover rate of γ-aminobutyric acid transporters. J Biol Chem 278:17716–17726

Yamashita A, Singh SK, Kawate T, Jin Y, Gouaux E (2005) Crystal structure of a bacterial homologue of Na^+/Cl^- dependent neurotransmitter transporters. Nature 437:215–223

Zampighi GA, Kreman M, Boorer KJ, Loo DDF, Bezanilla F, Chandy G, Hall JE, Wright EM (1995) A method for determining the unitary functional capacity of cloned channels and transporters expressed in *Xenopus laevis* oocytes. J Membr Biol 148:65–78

Zampighi GA, Loo DDF, Kreman M, Eskandari S, Wright EM (1999) Functional and morphological correlates of connexin50 expressed in *Xenopus laevis* oocytes. J Gen Physiol 113:507–523

Zhang Y, Hamill OP (2000) On the discrepancy between whole-cell and membrane patch mechanosensitivity in *Xenopus* oocytes. J Physiol 523:101–115